# SARS-CoV-2 infection of human pluripotent stem cell-derived vascular cells reveals smooth muscle cells as key mediators of vascular pathology during infection

Alexsia Richards[1#], Andrew Khalil[1,2,3#], Max Friesen[1], Troy W. Whitfield[1], Xinlei Gao[1],Tenzin Lungjangwa[1], Roger Kamm[4,5], Zhengpeng Wan[4], Lee Gehrke[6,7,8], David Mooney[3,6,+,*], Rudolf Jaenisch[1,8,+,*]

[1]Whitehead Institute for Biomedical Research, Cambridge, MA 02127

[2]Wyss Institute for Biologically Inspired Engineering, Harvard University, Boston, MA 02115

[3]John A. Paulson School of Engineering and Applied Sciences, Harvard University, Cambridge, MA, 02138

[4] Department of Biological Engineering, Massachusetts Institute of Technology, Cambridge, MA, 02127

[5]Department of Mechanical Engineering, Massachusetts Institute of Technology, Cambridge, MA, 02127

[6]Department of Microbiology, Harvard Medical School, Boston, MA 02115

[7] Institute for Medical Engineering and Science, Massachusetts Institute of Technology, Cambridge, MA, 02127

[8]Department of Biology, Massachusetts Institute of Technology, Cambridge, MA, 02127

[#] These authors contributed equally

[+] These authors jointly supervised this work

*Correspondence: mooneyd@seas.harvard.edu, jaenisch@wi.mit.edu

**Abstract**

Although respiratory symptoms are the most prevalent disease manifestation of infection by Severe Acute Respiratory Syndrome Coronavirus 2 (SARS-CoV-2), nearly 20% of hospitalized patients are at risk for thromboembolic events. This prothrombotic state is considered a key factor in the increased risk of stroke, which is observed clinically during both acute infection and long after symptoms clear. Here we develop a model of SARS-CoV-2 infection using human-induced pluripotent stem cell-derived endothelial cells (ECs), pericytes (PCs), and smooth muscle cells (SMCs) to recapitulate the vascular pathology associated with SARS-CoV-2 exposure. Our results demonstrate that perivascular cells, particularly SMCs, are a susceptible vascular target for SARS-CoV-2 infection. Utilizing RNA sequencing, we characterize the transcriptomic changes accompanying SARS-CoV-2 infection of SMCs, PCs, and ECs. We observe that infected SMCs shift to a pro-inflammatory state and increase the expression of key mediators of the coagulation cascade. Further, we show human ECs exposed to the secretome of infected SMCs produce hemostatic factors that contribute to vascular dysfunction, despite not being susceptible to direct infection. The findings here recapitulate observations from patient sera in human COVID-19 patients and provide mechanistic insight into the unique vascular implications of SARS-CoV-2 infection at a cellular level.

65 **Introduction**

66 Over the past 20 years, human coronaviruses have been responsible for severe outbreaks worldwide,
67 including the Severe Acute Respiratory Syndrome (SARS) outbreak of 2003 and the Middle East
68 Respiratory Syndrome (MERS) outbreak of 2012[1]. Most recently, the global pandemic caused by the
69 Severe Acute Respiratory Syndrome Coronavirus 2 (SARS-CoV-2) has led to over 700 million
70 documented cases and nearly 7 million deaths as of January 2023[2]. Although the primary symptoms
71 of SARS-CoV-2 infection are associated with the respiratory system, severe illness is also associated
72 with devastating vascular complications[3]. The most notable of these complications is a shift to a
73 prothrombotic state, with 20% of hospitalized patients reporting thromboembolic events and an
74 increased risk for blood clot-related issues, such as heart attack and stroke, which can last up to a year
75 after infection[4-7]. The frequency of these complications during and after SARS-CoV-2 infection is
76 significantly higher than after infection with other respiratory viruses, suggesting this pathology is
77 induced by effectors unique to SARS-CoV-2[8].

78 Indicators of endothelial cell (EC) activation and dysfunction, such as oxidative stress,
79 hyperpermeability, endothelial-to-mesenchymal transition (EndoMT), hypercoagulability, and
80 thrombosis have all been observed in SARS-CoV-2 infected patients [3]. However, *in vivo* direct infection
81 of ECs remains controversial[9, 10]. Infection has, however, been detected in epithelial cells in the lower
82 respiratory tract as well as vascular smooth muscle cells and pericytes[11-13]. Previous studies have
83 shown that the infection of respiratory epithelial cells triggers a cascade of inflammatory responses,
84 involving macrophages and monocytes, which can lead to widespread endothelial damage and
85 dysfunction[8, 14]. Additionally, these immune cells can secrete a variety of pro-inflammatory cytokines
86 and chemokines that exacerbate endothelial cell activation and dysfunction[15, 16]. It is likely the infection
87 or activation of multiple cell types in close proximity contributes to endothelial dysfunction.

88 Blood clot initiation begins with endothelial cells through both extrinsic and intrinsic pathways. The
89 extrinsic pathway is initiated through tissue factor expression in perivascular cells, including smooth

90 muscle cells. In addition, recently published data demonstrate that vascular smooth muscle cells are
91 crucial mediators of endothelial cell function [17, 18]. Here, the extensive crosstalk between vascular
92 endothelial cells and adjacent SMCs prompted us to examine if infection of SMCs cells could be the
93 trigger for the endothelial cell dysfunction and thromboembolic events associated with infection.

94 In this report, we built off previously published approaches[19, 20] to generate a new protocol to produce
95 uniform populations of ECs and perivascular cells, including SMCs and pericytes (PCs) from human
96 pluripotent stem cells (hPSCs). We specifically developed this approach using a serum-free and
97 common defined media for all three cell types to isolate the effects of culture conditions away from the
98 cellular responses to SARS-CoV-2. Using these cells, we modeled SARS-CoV-2 vascular infection
99 under defined conditions and investigated the cell-type specific response of vascular cells to SARS-
100 CoV-2 exposure. Our results show a preferential tropism for perivascular cells over ECs and that SMCs
101 are likely potent sites of SARS-CoV-2 infection. In addition, exposure to SARS-CoV-2 transforms SMCs
102 into activators of coagulation signaling in ECs which may, in turn, contribute to the devastating vascular
103 complications observed with SARS-CoV-2 infection in human patients. Finally, our system provides a
104 physiologically relevant platform for further studies on drug development and modeling vascular
105 pathogenesis in a defined system.

## 106 Results
107

### 108 A fully defined, efficient, and serum-free protocol allows for differentiation, culture, and
### 109 maintenance of ECs, PCs, and SMCs from hPSCs with a single common medium.

110 We established a step-wise protocol to generate and maintain both perivascular cells (PC and SMC)
111 and ECs in high purity (>97%) using a defined media (Fig. 1A-F). Similar to previously published
112 approaches[19, 20], the approach to generate ECs begins with mesendoderm specification using
113 CHIR99021-mediated WNT activation and bone morphogenetic protein 4 (BMP4), followed by
114 endothelial specification using vascular endothelial growth factor (VEGF), forskolin, and inhibition of

115 platelet-derived growth factor receptor (PDGFR) and transforming growth factor beta (TGFβ) signaling,
116 and a last stage of purification with n-cadherin inhibition, and continued PDGFR and TGFβ inhibition,
117 and maturation with sphingosine-1-phosphate (S1P) (Fig. 1A, Supplemental Fig. 1A-B). Alternatively,
118 after mesendoderm and early vascular specification, platelet-derived growth factor (PDGF-BB) addition
119 with TGFβ inhibition or TGFβ addition with PDGFR inhibition allowed for the derivation of PCs and
120 SMCs (Fig. 1B-E), respectively, in the same culture medium comprised of vascular base media
121 comprising of Gibco Vascular SFM™, heparin, B27, epithelial growth factor (EGF), basic fibroblast
122 growth factor (bFGF), and L-ascorbic acid-2-phosphate. All cells could be maintained and freeze-thaw
123 recovered in the same common medium with the addition of PDGF-BB for PCs and VEGF for ECs.

124 For ECs, these steps resulted in >85% purity as measured by VE-Cadherin (VE-Cad/CD144) and
125 PECAM1 (CD31) (Fig. 1D, Supplemental Fig. 1C), which could be enriched further via FACS and
126 maintained after recovery to greater than 98% purity (Fig. 1D, Supplemental Fig. 1C). In addition, the
127 ECs expressed canonical endothelial-related genes at levels similar to primary endothelial cells (Fig.
128 1B, Supplemental Fig. 1I). Our hPSC-ECs also expressed elevated levels of embryonic-restricted ETS
129 variant transcription factor 2 (ETV2), a critical transcriptional factor expressed by endothelial cells
130 specifically during vasculogenesis before capillary networks are formed[21], relative to HUVECs or the
131 starting hPSC population (Supplemental Fig. 1C). SMCs and PCs are two perivascular cell types that
132 have been previously classified as contractile and non-contractile perivascular cells and characterized
133 as both being PDGR positive. The delineation between the two is made through high or low levels of
134 expression of smooth muscle actin (SMA)[19, 22, 23] (Fig. 1D-E). Similarly, we captured these differences
135 via gene expression in the two perivascular cell populations derived here with higher levels of
136 contractile-related genes ACTA2 and CNN1 in SMCs and higher levels of PDGFRa and angiopoietin-
137 1 (ANGPT1) in PCs (Fig. 1B). PC expression of PDGFRb, PDGFRa as well as the expression of the
138 vascular adhesion molecules VCAM1 and ICAM1 was similar to levels observed in primary PCs
139 (Supplemental Fig.1I). To further characterize our hPSC-derived vascular cell populations we
140 performed principal component analysis (PCA) comparisons of these cell populations to each other

141 and the primary cell counterparts (Fig. 1C). These results show that the stem cell-derived ECs group
142 with HUVECs, while the stem cell-derived SMCs and pericytes cluster with bronchial SMCs and primary
143 pericytes. We then further resolved the mural cell populations in separate PCA analyses without hPSCs
144 and ECs (Fig. 1C). Euclidean distance comparisons showed that hPSC-SMCs are closer to BSMCs
145 and hPSC-PCs to primary brain vascular pericytes (Supplemental Fig. 1G-H).

146 Additionally, immunohistochemistry of PCs and SMCs showed lower levels of expression in SMA and
147 higher levels of NG2 and PDGFRb in PCs relative to SMCs (Fig. 1D-E). Importantly, relative to
148 previously published protocols[19, 20], both of these perivascular cells were derivable in high purity
149 (>97%), as shown in Fig. 1D-E and Supplemental Figs. 1E-F. PCs additionally expressed intermediate
150 levels of both PDGFRa and PDGFRb relative to fibroblasts and the starting hPSC population Fig. 1E
151 and Supplemental Figs. 1E-F. We also examined the ability of our hPSC-derived PCs and SMCs to
152 support microvascular network (MVN) formation with hPSC-derived ECs. Our results show that both
153 cell populations closely associated with hPSC-EC vascular networks (Supplemental Fig. 1J). Taken
154 together, the Euclidean distance measurements with PDGFRα/β expression comparison of the hPSC-
155 derived SMCs and PCs to their primary cell counterparts, the examination of perivascular-specific
156 genes such as ANGPT1, and their ability to support in vitro vascular formation collectively help to
157 establish the authentic identity of the hPSC-derived mural cells (Fig. 1C-E & Fig. 1G-J) . Furthermore,
158 this parallel derivation in the same serum-free and defined base media specifically allowed for the
159 comparative infection studies in one common infection medium without the confounding variables of
160 different or undefined media formulations.

161 **SARS-Cov-2 demonstrates preferential tropism for human perivascular cells.**

162 To assess the potential of hPSC-derived SMCs, PCs, and ECs to be infected by SARS-CoV-2, we
163 exposed the differentiated cells to live SARS-CoV-2 and collected media at 24 and 48 hours post-
164 exposure. We quantified the amount of infectious virus via plaque assays and found increased
165 infectious virus in the media from SMCs and PCs, indicating that both cell types were productively

166 infected with SARS-COV-2 (Fig. 2A). Notably, SMCs showed the highest amount of released virus over
167 a 48-hour infection (Fig. 2A). Conversely, exposure of ECs to SARS-CoV-2 resulted in no subsequent
168 release of infectious virus in the media, suggesting that these cells are not productively infected with
169 SARS-CoV-2 (Fig. 2A). Double-stranded RNA (dsRNA) is produced during SARS-CoV-2 genome
170 replication[24]. In agreement with the plaque assay data, we detected dsRNA in a subset of hPSC-derived
171 PCs and SMCs, indicating active viral replication, but not in ECs (Fig. 2B). To further confirm that ECs
172 were not productively infected by SARS-CoV-2, we quantitated both positive- and negative-sense viral
173 genome copies in ECs following exposure to SARS-CoV-2. The negative-sense genome copy is
174 generated specifically during viral replication and thus should not be present in the input virus[24]. Our
175 data showed that in ECs exposed to live SARS-CoV-2, levels of both positive- and negative-sense viral
176 genomes were comparable to those in ECs exposed to heat-inactivated virus (Supplemental Fig. 3A),
177 strongly suggesting an absence of active infection. In contrast, smooth muscle cells (SMCs) exhibited
178 robust replication, with significantly increased levels of both positive- and negative-sense copies only
179 after exposure to live SARS-CoV-2, and not to heat-inactivated virus (Supplemental Fig. 3A).
180 Collectively, these data support published reports that primary endothelial cells are likely not primary
181 targets of SARS-CoV-2 infection[9]. To determine if the expression of known SARS-CoV-2 receptors
182 could account for the observed differences in tropism between hPSC-derived SMCs, PC, and ECs we
183 examined the expression of ACE2, TMPRSS2, and NRP1 which have all been reported to contribute
184 to SARS-CoV-2 entry[25, 26]. Expression of ACE2 and TMRPSS2 was higher in SMCs, and PCs, relative
185 to ECs (Fig. 2C). ECs showed the highest expression of NRP1 amongst the three cell types (Fig 2C).
186 This result was perhaps not surprising given the known role of NRP1 in endothelial angiogenesis[27].
187 NRP1 can also bind to the SARS-CoV-2 Spike protein. Critically, previous studies have shown that the
188 expression of NRP1 alone is not sufficient to make cells susceptible to SARS-CoV-2 infection[26]. These
189 data suggest that the expression of ACE2 and TMPRSS2 may contribute to the increased susceptibility
190 of SMCs and PCs to SARS-CoV-2 infection. The striking differences in the susceptibility of SMCs, PCs

191 and ECs to SARS-CoV-2 infection prompted us to compare the transcriptional response of these cell
192 types to SARS-CoV-2 exposure.

193 **SARS-CoV-2 exposure drives divergent transcriptomic responses in human SMCs, PCs and**
194 **ECs**

195 To identify the transcriptional changes induced by SARS-CoV-2 infection, we performed bulk RNA
196 sequencing on hPSC-derived ECs, PCs and SMCs exposed to SARS-CoV-2. Although our results
197 showed that ECs are not productively infected with SARS-CoV-2, previous reports have demonstrated
198 that exposure to SARS-CoV-2 proteins is sufficient to impair EC function[28]. In the model developed
199 here, human ECs, PCs, and SMCs exposed to live SARS-CoV-2 showed significant changes in gene
200 expression (Fig. 3A-C). Notably, only SMCs showed a strong induction of inflammatory signaling
201 pathways following exposure to live SARS-CoV-2 (Fig 3B), ECs showed a strong upregulation of genes
202 relating to reactive oxygen species production (Fig 3A). Surprisingly, PCs exposed to SARS-CoV-2
203 showed a unique transcriptional profile with few pathways significantly upregulated in infected PCs (Fig
204 3C).

205 The vascular complications associated with SARS-CoV-2 infection were most significant following
206 infection with the WA-1/2020 strain of SARS-CoV-2, while later variants, which appeared in the spring
207 of 2022 were associated with less severe clinical outcomes[29]. To determine if reduced activation of
208 innate immune signaling in SMCs could contribute to these differences we examined the transcriptional
209 response of SMCs to infection with the Omicron BA5.1 variant of concern (VOC). BA5.1 infection of
210 SMCs induced inflammatory signaling, however, the enrichment of interferon-α and interferon-γ
211 response pathways was reduced relative to the induction following infection with the WA-1/2020 strain
212 of SARS-CoV-2 (Fig. 3A, Supplemental Fig. 2).

213 To identify transcriptional changes unique to productive infection with SARS-CoV-2 we compared the
214 transcriptional response of ECs and SMCs following exposure to live SARS-CoV-2 or heat-inactivated

215 SARS-CoV-2. Heat inactivation has previously been shown to disrupt the SARS-CoV-2 virion resulting
216 in a non-infectious, but intact virion[30]. In ECs the changes in gene expression appeared to primarily
217 reflect their response to SARS-CoV-2 virions, as there were few differentially expressed genes in EC
218 exposed to live vs. heat-inactivated (HI) SARS-CoV-2 (Supplemental Fig.3A). We do observe that in
219 ECs exposed to live SARS-CoV-2 compared to those exposed to heat-inactivated SARS-CoV-2 there
220 is a positive enrichment of gene sets associated with metabolic processes (e.g. oxidative
221 phosphorylation, adipogenesis, and cholesterol homeostasis), cell cycle (Myc targets), and cell death
222 (DNA repair) pathways. (Supplemental Fig. 3A). Although we see no evidence of productive infection
223 of ECs by SARS-CoV-2 it is possible that heat-inactivation alters the conformation of viral proteins in a
224 way that reduces their potential to activate these pathways in ECs. Similarly, treatment with free viral
225 spike and nucleocapsid proteins alone was also not able to recapitulate the activation of metabolic, cell
226 cycle, or cell death pathways observed following exposure to live SARS-CoV-2 (Supplemental Fig. 3B).

227 SMCs responded more significantly to live SARS-CoV-2 infection with respect to differentially
228 expressed genes, with, as expected, SARS-CoV-2 RNA being enriched in the infected SMC
229 upregulated genes (Supplemental Fig. 4A). SMCs exposed to live SARS-CoV-2 showed a robust
230 enrichment in the interferon-$\alpha$ and interferon-$\gamma$ innate immune response pathways compared to SMCs
231 exposed to heat-inactivated SARS-CoV-2 (Supplemental Fig. 4B) suggesting that productive infection
232 amplifies inflammatory signaling. Robust inflammatory signaling continued to be observed even at 72
233 hours after exposure to live SARS-CoV-2 (Supplemental Fig. 4C), further supporting the hypothesis
234 that the observed inflammatory response was due to prolonged infection and not only the result of initial
235 activation by extracellular viral particles.

236 To confirm the finding that EC exposure to SARS-CoV-2 increased the generation and response to
237 reactive oxygen species (ROS), ECs were then incubated with CellROX Green Reagent to detect the
238 generation of ROS by immunofluorescence. A significant increase in ROS signal was detected in ECs
239 exposed to both live and heat-inactivated SARS-CoV-2 for 48 hours (Fig. 4A-B). Induction of ROS has

240 the potential to increase vascular permeability[31]. To determine if exposure to SARS-CoV-2 reduced
241 endothelial cell barrier function, we measured permeability to FITC-dextran at 48 hours post-infection
242 (Fig. 4C). 10-kDa FITC–tagged dextran was added into the apical Transwell chamber, and
243 accumulation into the lower chamber was quantified. Our results showed that exposure to live SARS-
244 CoV-2 resulted in nearly a 50% increase in dextran release to the lower chamber (Fig 4C). Collectively,
245 these data both support our initial finding that SMCs are the susceptible vascular cell to SARS-CoV-2
246 infection as well as further show that infection and the presence of virions amplifies the divergent
247 responses in ECs and SMCs, specifically of reactive oxygen species and induction of innate immune
248 signaling respectively.

249 **SMC-secreted factors induce inflammatory signaling in ECs**
250
251 As shown in our data above, exposing hPSC-derived ECs directly to SARS-CoV-2 virions did not induce
252 significant innate immune signaling (Fig. 3A, and Supplemental Fig. 3A). However, elevated
253 inflammatory signaling is a key component of endothelial cell activation observed during SARS-CoV-2
254 infection[3]. We have demonstrated here that SMCs are a target for SARS-CoV-2 infection, and the
255 crosstalk between SMCs and ECs has been previously shown to contribute to the pathology of vascular
256 disease[17]. We hypothesized that ECs could be impacted by factors secreted by nearby infected SMCs.
257 To test this hypothesis, we exposed ECs to media collected from infected SMCs (CoV-2 SMC CM)
258 (Fig. 5A). In addition, we collected media from SMCs exposed to HI SARS-CoV-2 (HI SMC CM) to
259 identify any changes in ECs that result from the SMC response to viral particles alone (Fig. 5A).
260 Exposure of ECs to either CoV-2 SMC CM or HI SMC CM resulted in significant changes in gene
261 expression when compared to control ECs (Fig. 5B-C, Supplemental Fig. 5).
262
263 We again performed GSEA and observed that both treatment conditions demonstrated induction of
264 pathways that could potentially contribute to vascular dysfunction via the effects on ECs by infected
265 neighboring perivascular cells such as SMCs. As before, we observed upregulation of genes
266 associated with reactive oxygen species (Fig. 5D-E); however, treatment with live or HI CoV-2 SMC

267 CM increased the normalized enrichment scores for this pathway. Unlike the direct infection effects
268 described in Fig. 3A,C and Supplemental Fig.3A, this model, which mimics the effect of SMC secreted
269 factors on ECs, now induced inflammatory signaling pathways in ECs, including IFN-α and IFN-γ
270 response pathways, and TNFα signaling via NF-κB (Fig. 5D-E, Supplemental Fig. 6). Notably, the
271 induction of many genes in the interferon response pathways was significantly higher in EC exposed
272 to CoV-2 SMC CM compared to EC exposed to HI SMC CM (Supplemental Fig. 7). Lastly, both transfer
273 conditions resulted in further upregulation of the previously observed metabolic pathways as well as an
274 increase in TGFβ-signaling known to regulate EndoMT[32, 33] and apoptosis (Fig. 5D-E). Notably,
275 exposure of ECs to SMC infection media without SMC conditioning did not result in induction of up-
276 regulation of the inflammatory or coagulation pathways we observed with SMC conditioned media
277 (Supplemental Fig. 8). To determine if factors secreted by SMCs infected with BA5.1 could also induce
278 an inflammatory response in ECs we performed similar experiments using BA5.1 SMC conditioned
279 media (BA5.1 SMC CM). While we did observe an upregulation in IFN-α and IFN-γ pathways in ECs
280 treated with BA5.1 SMC CM, the differential expression of many of the key regulators of the innate
281 immune response that we observed as upregulated following exposure to CoV-2 SMC CM was
282 significantly reduced in treatment with BA5.1 SMC CM (Supplemental Figure S9, Table 1).
283
284 SARS-CoV-2 productively infected pericytes; however, we did not observe induction of inflammatory
285 signaling following infection (Fig. 3C). To determine whether factors secreted from SARS-CoV-2
286 infected pericytes induced inflammatory signaling in ECs we performed a parallel experiment using
287 media conditioned by pericytes exposed to SARS-CoV-2 (CoV-2 PC CM). We observed enrichment in
288 IFN-α and IFN-γ response pathways in CoV-2 PC CM exposed ECs compared to control ECs
289 (Supplemental Fig. 10); however, with the exception of HELZ2 none of the major mediators of
290 inflammatory signaling that we observed upregulated in ECs treated with CoV-2 SMC CM were
291 significantly upregulated in ECs treated with CoV-2 PC CM (Table 1, Supplemental Fig. 6, and
292 Supplemental Fig. 10B). Taken together, these data indicate that, while no substantial responses

293 outside of increased reactive oxygen species-related gene signaling were detected after direct
294 exposure, ECs can be impacted by factors released from nearby, infected perivascular cells. In
295 particular, we observed upregulation in pathways with a potential connection to vascular dysfunction
296 (innate immune signaling, metabolic disruption, TGFβ-signaling, and cell death) in response to SMC-
297 and PC-secreted factors.

298
299
300 **SMC-secreted factors increase the expression of known coagulation pathways in ECs**

301 In addition to the enriched pathways described above, we also observed that exposing ECs to media
302 from infected or HI-exposed SMCs significantly upregulated the expression of multiple genes involved
303 in coagulation (Fig. 5D-E and 6A-B). Included in the coagulation gene set[34] was SERPINE1, a known
304 inhibitor of plasminogen (PA-1) and a blood biomarker of which elevated plasma levels have been
305 observed in patients with severe SARS-CoV-2 infection[35] (Fig. 6A-B). To determine if the exposure of
306 ECs to media from infected SMCs also increased protein secretion, we measured SERPINE1 protein
307 levels in the media from ECs exposed to SARS-CoV-2 infected SMCs for 48 hours (CoV-2 SMC-
308 Exposed). CoV-2 SMC-exposed ECs released significantly more SERPINE1 than ECs exposed to
309 media from mock-infected SMCs (Mock SMC Exposed) (Fig. 6C). Similar to SERPINE1, increased
310 plasma levels of von Willebrand Factor (vWF), a blood glycoprotein involved in clotting released from
311 activated ECs and a common biomarker for coagulopathies[36], has been observed in patients with
312 severe SARS-CoV-2 infection[35, 37]. ECs exposed to media from SARS-CoV-2 infected SMCs (CoV-2
313 SMC Exposed) also released significantly more vWF into the media than ECs exposed to media from
314 mock-infected SMC media (Mock SMC Exposed) (Fig. 6D). Interestingly, ECs exposed to media from
315 BA5.1 infected SMCs did not show significant upregulation of the coagulation gene set compared to
316 control ECs (Supplemental Fig. 9A). In addition, we observed no significant release of vWF or
317 SERPINE1 into the media in ECs exposed to conditioned media (CM) from BA5.1 infected SMCs
318 relative to ECs that had been exposed to CM from mock infected SMCs. (Supplemental Fig. 11).
319 Although ECs exposed to media from SARS-CoV-2 infected PCs did show an increased expression of

genes within the coagulation gene set (Supplemental Fig. 10A), we did not observe increased release of vWF or SERPINE1 into the media following exposure to CoV-2 PC CM (Supplemental Fig. 12). We propose that these data suggest that the observed coagulopathy-related vascular dysfunction observed in human patients infected with SARS-CoV-2 may be related, in part, to the paracrine effects induced by neighboring infected SMCs and the resulting increased prothrombotic signaling from ECs.

Infection of SMCs with SARS-CoV-2 results in significant induction of IFN-α and IFN-γ signaling pathways (Fig. 3, Supplemental Fig. 4). To determine if activation of these inflammatory pathways could contribute to the release of factors that promote activation of coagulation pathways in ECs, SMCs were treated with IFN-α or IFN-γ for 24 hours. The media was then replaced with fresh media without cytokines for 48 hours, at which point the media was collected. ECs were then incubated with IFN-α or IFN-γ SMC-conditioned media and the levels of vWF or SERPINE1 released into media were quantitated relative to ECs treated with media conditioned by untreated SMCs or PCs. ECs exposed to media from IFN-α treated SMCs showed a significant increase in the release of vWF as well as increased release of SERPINE1 (Supplemental Fig. 13A). We performed similar experiments using media conditioned by IFN-α or IFN-γ treated PCs. Treatment of ECs with media from IFN-α or IFN-γ PCs did not cause an increase in release of vWF or SERPINE1 (Supplemental Fig. 13B). Collectively, these findings suggest that activation of inflammatory signaling in SMCs may contribute to the release of factors that promote activation of coagulation cascades in ECs.

**Infected SMCs release factors that increase brain microvascular endothelial cell permeability**

A recent study has shown disruption of the blood-brain barrier in patients during acute SARS-CoV-2 infection as well as in patients suffering from long COVID cognitive impairment [38]. hPSC-derived brain microvascular endothelial cells (hBMECs) recapitulate much of the unique physiology of the brain microvascular endothelial cells in the blood-brain barrier [39, 40]. As we observed clear dysfunction in the more peripheral-like ECs after exposure to factors secreted by infected perivascular cells, we modeled

346 exposure of hBMECs to factors released from infected perivascular cells. Similar to the peripheral ECs,
347 hBMECs exposed to live virus for 24 or 72 hours and stained with an antibody against dsRNA showed
348 little to no infection, indicated by rare dsRNA-positive cells at the 72-hour time point (Supplement Fig.
349 14A). These data are in agreement with a previous report that showed a low level of infection by 72
350 hours in primary BMECs[41]. As our findings here have indicated (Fig. 5D and Supplemental Fig. 6)
351 infected SMCs release factors that promote inflammatory signaling in ECs, we hypothesized that similar
352 signaling would result in decreased barrier integrity in hBMECs. Transendothelial electrical resistance
353 (TEER) provides a quantitative measurement of junctional tightness[42]. TEER was measured in
354 hBMECs that were plated in transwell plates and exposed to media from either mock-infected SMCs
355 (Mock CM-Exposed) or SMCs infected with live SARS-CoV-2 (CoV-2 SMC-Exposed) or heat-
356 inactivated SARS-CoV-2 (HI SMC Exposed) over the course of 72 hours. We observed a significant
357 reduction in TEER values over time in CoV-2 SMC Exposed hBMECs (Supplemental Fig. 14B),
358 whereas no reduction was observed in HI SMC Exposed hBMECs (Supplemental Fig. 14C).

359 **hPSC-derived SMCs increase tissue factor expression and activity in response to SARS-CoV-2**
360 **infection and constitute a platform for identifying targeted antiviral therapies**

361 Tissue factor (TF) is a key initiator of the extrinsic blood coagulation pathway expressed in vascular
362 smooth muscle cells following injury[43], and in the lungs of patients with severe SARS-CoV-2 infection[44,
363 45]. To determine if SARS-CoV-2 infection of SMCs resulted in increased TF expression, SMCs were
364 exposed to either live SARS-CoV-2 or heat-inactivated SARS-CoV-2 and stained with an antibody
365 against TF. Exposure to live SARS-CoV-2 resulted in an increase in TF staining in SMCs (Fig. 7A-B),
366 which appeared to correlate with dsRNA positive cells (Supplemental Fig. 15). Quantifying the average
367 intensity of SMCs expressing TF, we observed that this increase was specific to live SARS-CoV-2
368 infection (Fig. 7C). To further determine whether the increased surface expression of TF indicated
369 functional activation, we employed an enzyme-linked immunosorbent assay (ELISA) to quantitate TF
370 activity from lysate of SMCs exposed to live or heat-inactivated SARS-CoV-2. We observed significantly
371 higher TF activity in the lysate from SMCs infected with SARS-CoV-2 (Fig. 7D). Collectively, these data

372 suggest that the upregulation of TF is a direct effect of infection and gives additional cellular mechanistic
373 insight into how SARS-CoV-2 infection and the tropism shown here might cause the unique vascular
374 dysfunction observed in COVID-19 patients.

375 Given that our data here suggest that infection of SMCs may be one of the major initiating factors in
376 the development of the vascular pathology associated with infection, we sought to determine whether
377 inhibiting known viral infection pathways in perivascular cells would blunt this as a proof-of-principle of
378 this model's use in drug development in infectious disease with vascular complications. The
379 sphingolipid synthesis pathway has been shown to play a critical role in the replication of viruses and
380 regulation of the innate immune response[46] and is involved in the development and maturation of blood
381 vessels[47, 48]. Modulation of this pathway has been proposed as a potential therapeutic treatment for
382 severe infection[49]. To determine if inhibition of sphingolipid signaling in SMCs could reduce SARS-
383 CoV-2 infection, SMCs were treated with N,N-Dimethyl-D-erythro-sphingosine (DMS), which inhibits
384 the phosphorylation of sphingosine to form sphingosine 1-phosphate. Treatment with DMS resulted in
385 a dose-dependent reduction of infectious virus production in SMCs, which could not be accounted for
386 by the toxicity of the drug (Supplemental Fig. 16A). We compared the transcriptional response of SARS-
387 CoV-2 infected SMCs with and without treatment with DMS during infection. We observed increased
388 activation of inflammatory pathways in DMS-treated SARS-CoV-2 infected SMCs, which may in part,
389 account for the reduced level of viral infection (Supplemental Fig. 16A-B). To determine if EC viability
390 was impacted by treatment with DMS at a concentration that reduced viral infection in SMCs while not
391 reducing SMC viability (Supplemental Fig. 16A), we additionally performed the CellTiter Glo viability
392 assay on ECs 72 hours after DMS exposure and observed no reduction in EC viability relative to control
393 DMSO exposed ECs (Supplemental Fig. 16C).

394 **Discussion**

395 The SARS-CoV-2 pandemic has impacted millions of people worldwide. The vascular complications
396 that arise from severe infection continue to devastate patients long after the peak of infection. One year
397 after infection, patients who were infected with SARS-CoV-2 are 63% more likely to have cardiovascular
398 issues and have a 52% increased risk of stroke[5]. In this report, we present a model system to study the
399 tropism and pathology associated with SARS-CoV-2 vascular infection. Our data demonstrate that
400 within the vasculature, perivascular cells, including pericytes and smooth muscle cells, are major
401 targets for SARS-CoV-2 infection. Also consistent with previous reports[9], our results here show no
402 evidence of productive viral infection in human ECs. These data are particularly relevant in light of
403 recent studies using patient biopsy samples that showed evidence of the spread of infection through
404 the bloodstream during an early viremic phase[12]. This systemic spread likely results in virus throughout
405 the body following infection of the respiratory tract[12].

406 To enable this study, we developed a new, defined, and serum-free protocol to derive endothelial cells
407 and multiple mural cell populations from hPSCs using a single common medium. This approach
408 produced high-purity vascular cells that expressed canonical markers corresponding to their respective
409 vascular identities[50]. Specifically, the perivascular cell populations, representing pericytes and smooth
410 muscle cells, exhibited varying levels of RNA expression of key markers such as PDGFR-A, PDGFR-
411 B, NG2, TAGLN, and SMA[50] While specific definitions of perivascular cell identities remain important
412 areas of investigation in vascular biology, critically, these cells were functionally capable of supporting
413 vascular network formation via hPSC-ECs when exposed to flow (Supplemental Fig. 1J) and expressed
414 specific makers associated with vessel support and maintenance such as ANGPT1 [51, 52](Fig. 1).
415 Moreover, PCA of RNA sequencing of these cells and Euclidean distance comparisons with their
416 primary counterparts showed that the SMCs clustered with primary bronchial smooth muscle cells and
417 PCs with primary pericytes, respectively (Fig. 1B). The additional criteria of generating these
418 populations of cells in a common and standardized defined medium for all cell types enabled the
419 comparisons between these cell types under uniform infection culture conditions and, combined with

420 the ability to form vascular networks in these defined conditions, collectively illustrate the utility of this
421 new derivation method for the broad study of vascular biology using human pluripotent stem cells.

422 While we did not observe any productive infection of ECs, the RNA seq data did show perturbation of
423 EC gene expression by exposure to SARS-CoV-2 (Fig. 3A), such as perturbations expression of in
424 EGF-like repeats and discoidin I-like domain genes that play a significant role in endothelial cell
425 adhesion and angiogenesis[53]. Specifically, our results showed that exposure of ECs to SARS-CoV-2
426 resulted in significant downregulation of EDIL3 (Fig. 3A). Consistent with this hypothesis, we observed
427 reduced EC barrier function following exposure to SARS-CoV-2 (Fig. 4C). To better understand the
428 direct effects on vascular endothelium from SARS-CoV-2 exposure in the absence of infection, we
429 exposed ECs to both live and HI SARS-CoV-2 particles. The absence of significant differences following
430 live versus HI exposure in ECs suggests the direct impact on vascular endothelium could be due to
431 interactions between ECs and the viral proteins present on the surface of the viral particle. This finding
432 is in line with a previous study in hamsters using pseudotyped virus expressing SARS-CoV-2 spike
433 protein[28]. Lastly, these effects were not observed with free recombinant nucleocapsid or spike protein,
434 indicating viral particle presentation of these proteins may be required (Supplemental Fig.3).

435 Our comparison of the transcriptional response in smooth muscle cells (SMCs) to live versus heat-
436 inactivated SARS-CoV-2 revealed the specific upregulation of several inflammatory genes, including
437 HELZ2, MX1, and IFI6, during active infection. These genes play key roles in orchestrating immune
438 responses to viral infections and are notably upregulated in patients with severe COVID-19[54-56]. The
439 selective elevation of these genes following exposure to live virus suggests that active SARS-CoV-2
440 infection enhances antiviral signaling in SMCs beyond what is triggered by viral proteins alone.

441 HELZ2, MX1, and IFI6 are also induced in endothelial cells (ECs) after exposure to factors secreted
442 from SARS-CoV-2-infected SMCs. Since ECs are not directly infected by SARS-CoV-2, this data
443 implies that inflammatory signals from neighboring SMCs are sufficient to activate expression in ECs.
444 All three genes are interferon-stimulated genes (ISGs), whose expression is induced by interferon (IFN)

445 signaling[57-59], we hypothesize that infected SMCs may secrete IFNs, which then activate these antiviral
446 pathways in nearby ECs.

447 Consistent with *in vivo* findings[60, 61], our data support perivascular cells as sites of active SARS-CoV-2
448 infection. An important question is how viral infection could spread from the initial site of infection in the
449 respiratory tract to perivascular cells in the absence of endothelial cell infection. During severe SARS-
450 CoV-2 infection the virus spreads systemically through the bloodstream to peripheral sites of infection.
451 Our data show weakened EC barrier function following exposure to SARS-CoV-2, which is consistent
452 with patient data as well as in vitro studies [8, 62, 63]. The specific observed reduction in EIDL3 levels in
453 our data suggests a possible specific mechanism where EC exposure to SARS-CoV-2 particles may
454 have the potential to impair barrier functions via weakened cell-cell adhesion and reduced
455 angiogenesis, contributing to extravascular dissemination of the virus during COVID19 and a route to
456 mural cell infection. We also observed the activation of ROS signaling in ECs following SARS-CoV-2
457 exposure, which may further contribute to reduced barrier function and increased vascular leakage.
458 Taken together, the results here demonstrate that EC exposure to SARS-CoV-2 elicits numerous
459 putative mechanisms of changes in gene expression and cellular function that lead to a reduction in
460 barrier integrity and provide an access point for the virus to contact perivascular cells and disseminate
461 into tissues, contributing to the collective understanding of COVID19 pathologies.

462 In identifying the sites of vascular infection, we also observed that only a subset of SMCs and PCs
463 were positive for dsRNA staining (Supplemental Fig. 1 & Supplemental Fig. 7). This may be due to
464 heterogeneity in receptor expression, or alternatively, the viral genomic replication that produces
465 dsRNA may be quickly dampened by the host cell's innate immune responses[64]. *In vivo,* it is likely that
466 only a small percentage of interactions between viral particles and cells result in productive infection
467 due to both the production of defective viral particles [65] as well as interactions of infectious viral particles
468 with cells that are not susceptible to SARS-CoV-2 infection. However, our results comparing the
469 transcriptional response of SMCs and ECs exposed to live virus versus heat-inactivated virus allowed

us to discriminate between transcriptional changes due to productive infection and changes induced via exposure to viral particles without downstream infection. Our results suggest that the overall SMC response may be sufficient to promote vascular dysfunction, and they prompted us to expand our model to mimic the exposure of ECs to factors released from infected SMCs.

Contrary to the limited dysfunction beyond endothelial ROS responses observed in our initial model of direct infection, the new model showed significant dysregulation of vascular gene pathways in ECs. Specifically, we observed increased expression of genes in interferon response pathways, further reactive oxygen species, and significant cell death in ECs exposed to the SMC-secreted milieu. Moreover, our RNA-seq data showed that SMCs exposed to heat-inactivated SARS-CoV-2 alone, which cannot initiate infection, release factors that promote coagulation signaling in ECs, suggesting that exposure of SMCs to circulating viral particles may be sufficient for activation of coagulation pathways through a SMC dependent mechanism. Lastly, the conditioned media model provided mechanistic insights into how neighboring SARS-CoV-2 infected perivascular cells can contribute to vascular dysfunction, such as leakage and edema through decreasing barrier function.

To assess the in vivo relevance of our model system, we explored several pathways that could underlie the vascular complications seen in COVID-19, such as hypercoagulability and bleeding disorders leading to exsanguination—events our data also detected[8, 35, 37, 66, 67]. Notably, we observed an upregulation of interferon-stimulated genes and coagulation mediators like SERPINE1 (encoding for plasminogen activator inhibitor-1) and vWF in ECs exposed to conditioned media from SARS-CoV-2-infected SMCs. These are both key factors known to mediate thromboembolic events[35] and have been observed at elevated levels in severe COVID-19 patients associated with high thrombotic risk[35, 37] suggesting fidelity of the model findings. In addition to this EC dysfunction driven by paracrine signaling, infected SMCs in our model showed increased Tissue Factor activity, a primary driver of the intrinsic coagulation cascade[43, 45], further aligning with in vivo reports of its upregulation in lung tissue from severe COVID-19 cases[45] and persistent systemic inflammation[44]. Beyond SMC-driven effects, our

495 model indicated that SARS-CoV-2 particles directly impair EC barrier function even without productive
496 infection, potentially explaining the paradoxical bleeding and exsanguination observed in severe
497 cases[66]. We identified significant disruptions in ROS signaling in ECs following viral exposure,
498 consistent with increased vascular permeability seen in severe COVID-19[63] and supported by elevated
499 NADPH oxidase activity in the microvasculature of patients[68]. Our concurrent observation of EIDL3
500 downregulation, with its potential role in weakening tight junctions and compromising vascular
501 integrity[53], suggests a novel mechanism by which SARS-CoV-2 may induce EC dysfunction. Given the
502 alignment of our collective findings with established observations in COVID-19 patients, further studies
503 using human vascular tissue are warranted to validate these possible EIDL3-dependent mechanisms.

504 The approach detailed here describes a highly efficient manner for deriving pure perivascular and
505 endothelial cells from hPSCs in a defined and common media for use in disease modeling. Using the
506 defined and serum-free conditions for all cell types, this model could be used to study the tropism of
507 SARS-CoV-2 on cells of the vasculature. The model and results described here add to the existing
508 literature that perivascular cells, not the endothelium, are the target sites of infection. However, viral
509 particles themselves can alter the state of ECs in the absence of infection. Additionally, the defined
510 common medium format for all cell types allowed us to perform a set of conditioned media experiments
511 without the complications of different media compositions and then probe the outcomes of changes in
512 the EC microenvironment from infection of neighboring perivascular cells. This approach ultimately
513 provided a potential intrinsic and extrinsic mechanism for coagulopathies associated with SARS-CoV-
514 2 and paradoxical vascular leakage and edema. In summary, our findings provide a highly efficient
515 derivation of a fully defined and serum-free hPSC vascular model and add to the knowledge of the
516 relationship between the unique vascular complications associated with SARS-CoV-2 infection and
517 COVID-19 patients.

518 **Methods**

519 **Ethics**

520 All research presented in this manuscript complied with all relevant ethical regulations involving the use
521 of human pluripotent stem cells and was approved by the Committee on the Use of Humans as
522 Experimental Subjects (COUHES) and assigned IRB protocol number #0612002068.
523
524 **hPSC lines and maintenance**
525 H1 (WA01) embryonic stem cells were obtained from WiCell. hPSCs were maintained in feeder-free
526 conditions in mTeSR Plus media (StemCell Technologies) on Matrigel (Corning) in 6-well tissue culture
527 dishes. For passaging, hPSCs were detached as clumps using Versene Solution (Thermo Fisher
528 Scientific) and replated at a ratio of 1:8-1:10.
529
530 **Directed differentiation of hPSCs to endothelial cells**
531 All media recipes are described in Supplemental Table 2. H1 hPSCs were cultured in E8 media
532 (Thermo Fisher Scientific) and dissociated using Accutase (Thermo Fisher Scientific) into a single cell
533 suspension and plated at 15,000 cells/cm$^2$ in E8 media with Y-27632 (10μM) and onto Matrigel-coated
534 tissue culture plates. Y-27632 was removed after 24 hours, and cells were cultured in E8 media until
535 they reached approximately 70% confluency, at which point the media was replaced with MelM media;
536 this is considered day 0. On day 2, the media was replaced with EC1 media. On day 5, the media was
537 replaced with EC2 media for 24 hours, and then cells were passaged 1:1 onto fibronectin (FC01010MG,
538 Fisher Scientific) coated tissue culture plates in EC3 media. Plates were coated with fibronectin at
539 10ug/ml for 30 minutes at 37°C prior to the addition of cells. After 48 hours, media was replaced with
540 EC4 media for 5 days and then sorted for VE-Cadherin and PECAM1 double-positive cells using FACS.
541 Sorted cells were plated back onto fibronectin and cultured for an additional 5 days in EC4 before
542 cryopreservation or extended expansion in EC5 medium.
543
544 **Directed differentiation of hPSCs to pericytes**

545 All media recipes are described in Supplemental Table 2. H1 hPSCs were cultured in E8 media
546 (Thermo Fisher Scientific) and dissociated using Accutase (Thermo Fisher Scientific) into a single cell
547 suspension and plated at 15,000 cells/cm$^2$ in E8 media with Y-27632 (10μM). Y-27632 was removed
548 after 24 hours and cells cultured in E8 media until they reached approximately 70% confluency at which
549 point the media was replaced with MelM media, this is considered day 0. On day 2 the media was
550 replaced with PC/SMC1 media. On day 5 the media was replaced with PC/SMC2 media for 24 hours
551 and then cells were passaged 1:3 on to fibronectin (FC01010MG, Fisher Scientific) coated tissue
552 culture plates in PC3 media. Plates were coated with fibronectin at 10ug/ml for 30 minutes at 37°C prior
553 to the addition of cells. After 48 hours media was replaced with PC4 media. After 48 hours the media
554 was replaced with fresh PC4 and cells kept in culture for 7 days prior to freezing.
555

556 **Directed differentiation of hPSCs to smooth muscle cells**

557 All media recipes are described in Supplemental Table 2. H1 hPSCs were cultured in E8 media
558 (Thermo Fisher Scientific) and dissociated using Accutase (Thermo Fisher Scientific) into a single cell
559 suspension and plated at 15,000 cells/cm$^2$ in E8 media with Y-27632 (10μM). Y-27632 was removed
560 after 24 hours and cells cultured in E8 media until they reached approximately 70% confluency at which
561 point the media was replaced with MelM media, this is considered day 0. On day 2 the media was
562 replaced with PC/SMC1 media. On day 5 the media was replaced with PC/SMC2 media for 24 hours
563 and then cells were passaged 1:3 on to fibronectin (FC01010MG, Fisher Scientific) coated tissue
564 culture plates in SMC3 media. Plates were coated with fibronectin at 10ug/ml for 30 minutes at 37°C
565 prior to the addition of cells. After 48 hours media was replaced with SMC4 media. After 48 hours the
566 media was replaced with SMC5 and cells kept in culture for 7 days prior to freezing.
567

568 **Directed differentiation of hPSCs to brain microvascular endothelial cells**

569 The differentiation of H1 hPSCs to brain microvascular endothelial cells was based on a previously
570 published protocols[39, 69, 70]. Briefly, hPSCs were dissociated using Accutase (Thermo Fisher Scientific)

571 into a single cell suspension and plated at 15,000 cells/cm$^2$ in StemFlex media with Y-27632 (10μM).
572 Y-27632 was removed after 24 hours and at 48 hours post-plating the media was replaced with
573 Unconditioned Media (UM) (100ml Knock-out Serum Replacement (Thermo Fisher Scientific), 5ml non-
574 essential ammino acids (Thermo Fisher Scientific), 2.5ml GlutaMax (Thermo Fisher Scientific), 5ml
575 Pen/Strep (Thermo Fisher Scientific), 3.5μl β-mercapto-ethanol (Sigma), and 392.5ml
576 DMEM/F12(1:1)), this was considered day zero. The media was replaced daily with fresh UM. On day
577 six the media was changed to hESFM (Thermo Fisher Scientific) supplemented with 20 ng/mL bFGF
578 (Peprotech), 10 μM retinoic acid (RA) (Sigma), and 1:50 B27 (Thermo Fisher Scientific). The media
579 was not changed for 48 hours. On day eight, cells were washed once with DPBS and incubated with
580 Accutase for 30 minutes at 37°C. Cells were collected via centrifugation and plated onto either standard
581 tissue culture plates or transwell plates (Corning #3460). Both plates and transwells were coated with
582 400 μg/mL collagen IV (Sigma Aldrich) and 100 μg/mL fibronectin (Fisher Scientific) overnight with
583 collagen and fibronectin and washed 1X with PBS prior to the addition of cells. For tissue culture plates,
584 cells were plated at a density of 250,000 cells/cm$^2$, whereas for transwell plates, cells were plated at a
585 density of 1.1 x $10^6$ cells/cm$^2$ on the transwell membrane. bFGF and RA were removed from the medium
586 24 hours after plating.
587
588 **Microvascular network formation**
589 3D cell culture chips (idenTx, AIM Biotech) were utilized to generate *in vitro* microvascular networks
590 (MVN)s. AIM chips contain three parallel channels: a central gel channel flanked by two media
591 channels. Microposts separate fluidic channels and serve to confine the liquid gelling solution in the
592 central channel by surface tension before polymerization. The gel channel is 1.3 mm wide and 0.25
593 mm tall, the gap between microposts is 0.1 mm, and the width of media channels is 0.5 mm. For
594 vascular cell seeding, hPSC (iPS11)-derived ECs and PCs or SMCs were co-seeded into the chip as
595 previously described[71]. Briefly, ECs and respective mural cells were concentrated in defined SFM
596 media minus heparin containing thrombin (4 U/mL). Cell mixture solution was then further mixed with

597 fibrinogen (3 mg/mL final concentration) at a 1:1 ratio and quickly pipetted into the chip through the gel
598 inlet with a final concentration of 6 x$10^6$/mL for ECs and 1.5 x$10^6$/mL for mural cells. The device was
599 placed upside down to polymerize in a humidified tip box and allowed to polymerize at 37 °C for 15 min
600 in a 5% $CO_2$ incubator, before endothelial serum free media was introduced to the media channels.
601 After seeding, culture medium was added and changed daily in the device. After 7 days, MVNs are
602 ready for further experiments.
603

604 **Cell characterization by bulk RNA sequencing and PCA**

605 Primary HUVEC cells were obtained from VWR (Cat# 10171-906). Primary bronchial smooth muscle
606 cells (BSMCs) were obtained from PromoCell (Cat# C12561). Primary pericytes were obtained from
607 ScienCell (Cat#1200). RNA was extracted using the RNeasy Plus Mini kit (QIAGEN) following the
608 manufacturer's protocol. For bulk RNA sequencing of total RNA, libraries were prepared using the Swift
609 RNA library prep kit (Swift Biosciences). RNA sequencing reads were mapped to the human genome
610 (version GRCh38) using the STAR aligner (version 2.7.1a)[72]. The mapped reads were assigned to the
611 human genes using featureCounts[73] with the parameters '-p -s 2', suitable for paired-end reversely-
612 stranded libraries. Before performing PCA on the 5000 most variable genes, the normTransform
613 function of DESeq2 (version 1.36.0)[74] was used to normalize, center and log-transform (with a
614 pseudocount of 1) the counts matrix. The 'prcomp' function in R (version 4.2.1) was used to carry out
615 the PCA. PC2 and PC3 were used for computing Euclidean distances for the BSMC comparison, while
616 PC1, PC2 and PC3 were used for the primary PC comparison. In the table of between-sample
617 Euclidean distances (shown in Source Data file) each column is a comparison samples within two
618 conditions. For computing pairwise Euclidean distances between pairs of conditions (Supplemental Fig.
619 1G-H) each group includes three replicates, so that there are 3 x 3 = 9 distance values corresponding to
620 all possible pairs. For making a heatmap visualization of the marker gene expression, the normalized
621 counts, $c_{ij}$, for gene *i* in cell type *j* was standardized as $z_{ij} = (-\mu_i)/\sigma_i$.
622

623 **SARS-CoV-2 propagation, titration, and inactivation**

624 SARS-CoV-2 (isolate USA_WA1/2020) was obtained from BEI Resources. BA.5.1 strain was obtained
625 from a clinical isolate through the MassCPR Variant Program and verified by whole genome
626 sequencing. The virus was propagated in Vero E6 cells (ATCC CRL-1586) cultured in Dulbecco's
627 modified Eagle's medium (DMEM) supplemented with 2% fetal calf serum (FCS), penicillin (50 U/mL),
628 and streptomycin (50 mg/mL). SARS-CoV-2 titer was determined in Vero E6 cells by plaque assay.
629 work with SARS-CoV-2 was performed in the biosafety level 3 (BSL3) at the Ragon Institute
630 (Cambridge, MA) following approved SOPs. To generate heat-inactivated SARS-CoV-2 a 1ml aliquot
631 of SARS-CoV-2 was heated to 85°C for 15 minutes. For infection of SMCs, PCs, or ECs the cell culture
632 media was removed and replaced with inoculating virus diluted in a minimum volume of culture media.
633 The cells were placed at 37°C for 1 hour at which point the inoculum was removed and replaced with
634 EC, PC, or SMC media or Infection media for conditioned media transfer experiments. For all
635 conditioned media experiments control ECs were treated with infection media (unconditioned) for 48
636 hours.

637

638 **Bulk RNA-sequencing of infected and exposed vascular cells**

639 ECs, SMCs or PCs were infected at an MOI of 1 or exposed to conditioned media. At the indicated time
640 of collection RNA was extracted using the RNeasy Plus Mini kit (QIAGEN) following the manufacturer's
641 protocol. For bulk RNA sequencing of total RNA, libraries were prepared using the Swift RNA library
642 prep kit (Swift Biosciences) or the SMARTerUltra-lowPOLYA-V4 (Takara Bio). Samples were
643 sequenced on a NovaSeq 6000 sequencer.

644

645 **Analysis of gene expression**

646 Paired-end reads (51x 51 bp) were mapped to a reference genome using the STAR aligner (v. 2.7.1a)[72].
647 The reference genome was a composite of the human genome (GRCh38) and that of the SARS-CoV-
648 2 coronavirus (GenBank MN988713.1). Counts for human protein coding genes and lncRNAs

649 (ENSEMBL release 93 annotations), together with the viral genes, were tabulated using
650 featureCounts[73]. Differential expression of mRNAs was assessed for pairwise contrasts between
651 conditions using estimated fold-changes and the Wald statistic in DESeq2 (v. 1.36.0)[74]. Per-gene
652 dispersions were estimated using all conditions, as within-condition variance was observed to be
653 relatively uniform across conditions in exploratory analyses. Unless otherwise noted, empirical Bayes
654 shrinkage was applied to fold-change estimates[75]. Gene-set enrichment analysis was carried out
655 between pairs of conditions using GSEA (v. 4.1.0)[76] with counts that were normalized by DESeq2 and
656 1000 gene-set permutations were used to estimate p-values. Gene-sets that were tested for enrichment
657 came from the Hallmark collection at the MSigDB[34].
658

659 **Flow cytometry**

660 HEK293T cells were obtained from ATCC and cultured in DMEM + 10% FBS and P/S, and split with
661 0.05% Trypsin for passaging. Human dermal fibroblasts (hDF) were obtained from Lonza and cultured
662 in DMEM + 10% FBS and P/S, and split with 0.05% Trypsin for passaging. For live surface marker
663 staining, cells were trypsinized with TrypLE Express for ~5-7 or until cells detached. Cells were washed
664 once with FACS staining buffer consisting of 2 mM EDTA and 0.5% BSA and centrifuged. Cells were
665 then resuspended and incubated in FACS staining buffer and the respective fluorophore-conjugated
666 antibodies for each cell type at the concentrations listed in Supplemental Table 1. For SMC staining
667 that included intracellular SMA, cells were fixed with 1% PFA after the trypsinization and washing step
668 listed above for 20 min at room temperature. The cells were then permeabilized in 90% methanol in
669 PBS at -20C for at least 24 hr. After permeabilization, cells were washed in FACS buffer and
670 resuspended in FACS buffer containing 0.1% Triton X-100 and the respective antibodies listed in
671 Supplemental Table 1. All antibodies were done for 20-30 min at 4C and were followed by a wash with
672 FACS buffer. Stained cells were analyzed on a BD Fortessa UV/Blue/Green/Red 4-laser flow
673 cytometer. Cells were isolated as a population and then selected for singlets before setting gates to
674 determine positive populations. Undifferentiated hPSCs served as biological controls for all stains.

675

676 **Immunofluorescence microscopy**

677 Cells were fixed with 4% paraformaldehyde for 15 minutes at room temperature. Fixed cells were
678 permeabilized for 15 minutes using 0.1% TX-100. Cells were then blocked with 3% BSA in PBS for 1
679 hour at room temperature. Cells were incubated with primary antibodies (see Supplemental Table 1)
680 diluted in antibody buffer (0.01%TX-100 and 1%BSA in PBS) overnight at 4°C. Cells were washed with
681 0.05% Tween in PBS and incubated for 1 hour at room temperature with secondary antibodies (see
682 Supplemental Table 1) diluted in antibody buffer. FITC-Phalloidin was added at 1:2000 and DAPI at
683 1:5000 with secondary antibodies.

684

685 **Imaging of reactive oxygen species production**

686 Endothelial cells were exposed to SARS-CoV-2 for 48 hours. At 48 hours post-infection the media was
687 removed and replaced with FluoroBrite media (A1896701, Thermo Fisher Scientific) supplemented with
688 1:50 B27 and CellRox Green Reagent (C10444, Thermo Fisher Scientific) at a final concentration of
689 5μM. Cells were incubated at 37°C for 30 minutes then washed 3 times with PBS and imaged
690 immediately after washing. Cells were kept in FluoroBrite with B27 throughout imaging. The average
691 intercellular florescence for five to seven cells for each condition was measured in each experiment.
692 Three independent experiments were performed.

693

694 **SERPINE1 (PAI-1) and von Willebrand factor (vWF) release measurements**

695 Endothelial cells (ECs) were exposed to media from SARS-CoV-2 infected or mock infected SMCs or
696 PCs for 48 hours at which point the media was collected and analyzed for PAI-1 content using the
697 Human Serpin E1/PAI-1 Quantikine ELISA Kit (DSE100, R&D Systems) according to the
698 manufacturer's protocol. The same media was analyzed for vWF content using the Human Von
699 Willebrand Factor ELISA Kit (ab223864, Abcam) according to the manufacturer's protocol. For analysis
700 on the impact of SMC or PC treatment with IFNα or IFNγ cells were plated in a 24-well plate and treated

701 with 100u/ml IFNα (ThermoFisher #111001) or 20ng/ml IFNγ(R&D 285-IF) in 300ul infection media for
702 24 hours at which point the cells were washed once with infection media and 300ul of fresh infection
703 added and collected again 24 hours after SMC or PC conditioning. ECs were then treated with this
704 conditioned media and the media was analyzed for vWF or SERPINE1 content as described above.
705

706 **Measurement of Tissue Factor Activity**

707 At 48 hours post-infection SMCs were lysed and solubilized with 50 mM Tris-buffered saline (pH 8.0)
708 containing 0.5% Triton X-100 or 0.1% Tween 20 at 4°C for 30 minutes. Samples were then centrifuged
709 at 10,000xg for 10 minutes, and the supernatant was collected for analysis. Tissue factor (TF) activity
710 was measured using a human tissue factor activity assay kit (ab108906, Abcam) according to the
711 manufacturer's protocol. Activity was normalized to total protein contents using the Pierce BCA Protein
712 Assay Kit (FERA65453, Thermo Scientific).
713

714 **Measurement of transendothelial electrical resistance**

715 BMECs were plated onto three Transwell filters (Corning #3460) using the procedure described in
716 "Directed Differentiation of hPSCs to brain microvascular endothelial cells" [69] .48 hours after plating the
717 media was removed from the apical side of the Transwell and replaced with SMC-conditioned media.
718 At each time point, the TEER was measured in three separate wells. All data are represented as mean
719 ± standard deviation for these collective measurements. Following the medium change on day 0 of
720 subculture to remove bFGF and RA, no further medium changes were performed for the duration of the
721 experiments.
722

723 **FITC-Dextran Permeability Assay**

724 Endothelial cells were seeded in 12-well Transwell plates (Corning #3460) at 5e5 cells/Transwell. 72
725 hours after seeding ECs were either infected with SARS-CoV-2 (MOI 1) or treated with SMC
726 conditioned media. 48 hours after treatment the media on the basolateral side was replaced with 1ml

727 of fresh EC media. FITC-tagged dextran (10 μM) was suspended in 0.5 ml of EC medium and added
728 to the apical side of the Transwell. To determine the level of transcytosis following 2 hours of incubation
729 in a 37°C incubator on a rotating platform, we collected 150 μl from the 1ml of EC medium on the
730 basolateral side of the Transwell. Fluorescence intensity in the collected media was measured using a
731 SpectraMax iD3 plate reader set to 495-nm excitation and 519-nm emission settings.
732
733 **CellTiter Glo Viability Assay**
734 Endothelial cells were plated in a 96 well plate at a density of 5e4 cells/well. 24 hours after plating the
735 media was replaced with EC media containing 1uM or 5uM DMS or a matched volume of DMSO. 72
736 hours after treatment a CellTiter Glo 2.0 (Promega # G9241) assay was performed according the
737 manufacturer instructions.
738

## 739 Data availability

740 The RNA sequencing data generated in this study has been deposited in the GEO database under
741 accession code GSE240766. All additional data generated in this study are provided in the
742 Supplementary Information/Source Data file.
743
744
745

## 746 References

747

748 1. Arora, P., Jafferany, M., Lotti, T., Sadoughifar, R. & Goldust, M. Learning from history: Coronavirus
749 outbreaks in the past. *Dermatol Ther* **33**, e13343 (2020).
750 2. WHO, Vol. 2021 (
751 3. Acharya, Y., Alameer, A., Calpin, G., Alkhattab, M. & Sultan, S. A comprehensive review of vascular
752 complications in COVID-19. *J Thromb Thrombolysis* **53**, 586-593 (2022).
753 4. Merschel, M. in American Heart Association News Stories, Edn. February 24, 2023 (2023).
754 5. Xie, Y., Xu, E., Bowe, B. & Al-Aly, Z. Long-term cardiovascular outcomes of COVID-19. *Nat Med* **28**,
755 583-590 (2022).

6. Spyropoulos, A.C. *et al.* Occurrence of Thromboembolic Events and Mortality Among Hospitalized Coronavirus 2019 Patients: Large Observational Cohort Study of Electronic Health Records. *TH Open* **6**, e408-e420 (2022).
7. Belani, P. *et al.* COVID-19 Is an Independent Risk Factor for Acute Ischemic Stroke. *AJNR Am J Neuroradiol* **41**, 1361-1364 (2020).
8. Ackermann, M. *et al.* Pulmonary Vascular Endothelialitis, Thrombosis, and Angiogenesis in Covid-19. *N Engl J Med* **383**, 120-128 (2020).
9. Schimmel, L. *et al.* Endothelial cells are not productively infected by SARS-CoV-2. *Clin Transl Immunology* **10**, e1350 (2021).
10. Urata, R. *et al.* Senescent endothelial cells are predisposed to SARS-CoV-2 infection and subsequent endothelial dysfunction. *Sci Rep* **12**, 11855 (2022).
11. McQuaid, C. & Montagne, A. SARS-CoV-2 and vascular dysfunction: a growing role for pericytes. *Cardiovasc Res* (2022).
12. Stein, S.R. *et al.* SARS-CoV-2 infection and persistence in the human body and brain at autopsy. *Nature* **612**, 758-763 (2022).
13. Ryu, G. & Shin, H.W. SARS-CoV-2 Infection of Airway Epithelial Cells. *Immune Netw* **21**, e3 (2021).
14. Varga, Z. *et al.* Endothelial cell infection and endotheliitis in COVID-19. *Lancet* **395**, 1417-1418 (2020).
15. Merad, M. & Martin, J.C. Pathological inflammation in patients with COVID-19: a key role for monocytes and macrophages. *Nat Rev Immunol* **20**, 355-362 (2020).
16. Blanco-Melo, D. *et al.* Imbalanced Host Response to SARS-CoV-2 Drives Development of COVID-19. *Cell* **181**, 1036-1045 e1039 (2020).
17. Lilly, B. We have contact: endothelial cell-smooth muscle cell interactions. *Physiology (Bethesda)* **29**, 234-241 (2014).
18. Mendez-Barbero, N., Gutierrez-Munoz, C. & Blanco-Colio, L.M. Cellular Crosstalk between Endothelial and Smooth Muscle Cells in Vascular Wall Remodeling. *Int J Mol Sci* **22** (2021).
19. Patsch, C. *et al.* Generation of vascular endothelial and smooth muscle cells from human pluripotent stem cells. *Nat Cell Biol* **17**, 994-1003 (2015).
20. Kumar, A. *et al.* Specification and Diversification of Pericytes and Smooth Muscle Cells from Mesenchymoangioblasts. *Cell Rep* **19**, 1902-1916 (2017).
21. Koyano-Nakagawa, N. & Garry, D.J. Etv2 as an essential regulator of mesodermal lineage development. *Cardiovasc Res* **113**, 1294-1306 (2017).
22. Cao, G. *et al.* How vascular smooth muscle cell phenotype switching contributes to vascular disease. *Cell Commun Signal* **20**, 180 (2022).
23. Wanjare, M., Kuo, F. & Gerecht, S. Derivation and maturation of synthetic and contractile vascular smooth muscle cells from human pluripotent stem cells. *Cardiovasc Res* **97**, 321-330 (2013).
24. Sola, I., Almazan, F., Zuniga, S. & Enjuanes, L. Continuous and Discontinuous RNA Synthesis in Coronaviruses. *Annu Rev Virol* **2**, 265-288 (2015).
25. Hoffmann, M. *et al.* SARS-CoV-2 Cell Entry Depends on ACE2 and TMPRSS2 and Is Blocked by a Clinically Proven Protease Inhibitor. *Cell* **181**, 271-280 e278 (2020).
26. Cantuti-Castelvetri, L. *et al.* Neuropilin-1 facilitates SARS-CoV-2 cell entry and infectivity. *Science* **370**, 856-860 (2020).
27. Fantin, A. *et al.* NRP1 acts cell autonomously in endothelium to promote tip cell function during sprouting angiogenesis. *Blood* **121**, 2352-2362 (2013).
28. Lei, Y. *et al.* SARS-CoV-2 Spike Protein Impairs Endothelial Function via Downregulation of ACE 2. *Circ Res* **128**, 1323-1326 (2021).
29. Wolter, N. *et al.* Early assessment of the clinical severity of the SARS-CoV-2 omicron variant in South Africa: a data linkage study. *Lancet* **399**, 437-446 (2022).
30. Loveday, E.K. *et al.* Effect of Inactivation Methods on SARS-CoV-2 Virion Protein and Structure. *Viruses* **13** (2021).
31. Boueiz, A. & Hassoun, P.M. Regulation of endothelial barrier function by reactive oxygen and nitrogen species. *Microvasc Res* **77**, 26-34 (2009).

32. Ma, J., Sanchez-Duffhues, G., Goumans, M.J. & Ten Dijke, P. TGF-beta-Induced Endothelial to Mesenchymal Transition in Disease and Tissue Engineering. *Front Cell Dev Biol* **8**, 260 (2020).
33. Cooley, B.C. *et al.* TGF-beta signaling mediates endothelial-to-mesenchymal transition (EndMT) during vein graft remodeling. *Sci Transl Med* **6**, 227ra234 (2014).
34. Liberzon, A. *et al.* The Molecular Signatures Database (MSigDB) hallmark gene set collection. *Cell Syst* **1**, 417-425 (2015).
35. Lopez-Castaneda, S. *et al.* Inflammatory and Prothrombotic Biomarkers Associated With the Severity of COVID-19 Infection. *Clin Appl Thromb Hemost* **27**, 1076029621999099 (2021).
36. Choudhary, S., Sharma, K. & Singh, P.K. Von Willebrand factor: A key glycoprotein involved in thrombo-inflammatory complications of COVID-19. *Chem Biol Interact* **348**, 109657 (2021).
37. Helms, J. *et al.* High risk of thrombosis in patients with severe SARS-CoV-2 infection: a multicenter prospective cohort study. *Intensive Care Med* **46**, 1089-1098 (2020).
38. Greene, C. *et al.* Author Correction: Blood-brain barrier disruption and sustained systemic inflammation in individuals with long COVID-associated cognitive impairment. *Nat Neurosci* **27**, 1019 (2024).
39. Stebbins, M.J. *et al.* Differentiation and characterization of human pluripotent stem cell-derived brain microvascular endothelial cells. *Methods* **101**, 93-102 (2016).
40. Helms, H.C. *et al.* In vitro models of the blood-brain barrier: An overview of commonly used brain endothelial cell culture models and guidelines for their use. *J Cereb Blood Flow Metab* **36**, 862-890 (2016).
41. Yang, R.C. *et al.* SARS-CoV-2 productively infects human brain microvascular endothelial cells. *J Neuroinflammation* **19**, 149 (2022).
42. Srinivasan, B. *et al.* TEER measurement techniques for in vitro barrier model systems. *J Lab Autom* **20**, 107-126 (2015).
43. Wang, L. *et al.* Vascular smooth muscle-derived tissue factor is critical for arterial thrombosis after ferric chloride-induced injury. *Blood* **113**, 705-713 (2009).
44. Nguyen, D., Jeon, H.M. & Lee, J. Tissue factor links inflammation, thrombosis, and senescence in COVID-19. *Sci Rep* **12**, 19842 (2022).
45. Subrahmanian, S. *et al.* Tissue factor upregulation is associated with SARS-CoV-2 in the lungs of COVID-19 patients. *J Thromb Haemost* **19**, 2268-2274 (2021).
46. Spiegel, S. & Milstien, S. The outs and the ins of sphingosine-1-phosphate in immunity. *Nat Rev Immunol* **11**, 403-415 (2011).
47. Yanagida, K. & Hla, T. Vascular and Immunobiology of the Circulatory Sphingosine 1-Phosphate Gradient. *Annu Rev Physiol* **79**, 67-91 (2017).
48. Schuchardt, M., Tolle, M., Prufer, J. & van der Giet, M. Pharmacological relevance and potential of sphingosine 1-phosphate in the vascular system. *Br J Pharmacol* **163**, 1140-1162 (2011).
49. McGowan, E.M., Haddadi, N., Nassif, N.T. & Lin, Y. Targeting the SphK-S1P-SIPR Pathway as a Potential Therapeutic Approach for COVID-19. *Int J Mol Sci* **21** (2020).
50. Vanlandewijck, M. *et al.* A molecular atlas of cell types and zonation in the brain vasculature. *Nature* **554**, 475-480 (2018).
51. Armulik, A., Genove, G. & Betsholtz, C. Pericytes: developmental, physiological, and pathological perspectives, problems, and promises. *Dev Cell* **21**, 193-215 (2011).
52. von Tell, D., Armulik, A. & Betsholtz, C. Pericytes and vascular stability. *Exp Cell Res* **312**, 623-629 (2006).
53. Niu, X. *et al.* EDIL3 influenced the alphavbeta3-FAK/MEK/ERK axis of endothelial cells in psoriasis. *J Cell Mol Med* **26**, 5202-5212 (2022).
54. Gajate-Arenas, M. *et al.* The Immune Response of OAS1, IRF9, and IFI6 Genes in the Pathogenesis of COVID-19. *Int J Mol Sci* **25** (2024).
55. Bizzotto, J. *et al.* SARS-CoV-2 Infection Boosts MX1 Antiviral Effector in COVID-19 Patients. *iScience* **23**, 101585 (2020).
56. Nain, Z. *et al.* Transcriptomic studies revealed pathophysiological impact of COVID-19 to predominant health conditions. *Brief Bioinform* **22** (2021).

57. Parker, N. & Porter, A.C. Identification of a novel gene family that includes the interferon-inducible human genes 6-16 and ISG12. *BMC Genomics* **5**, 8 (2004).
58. Mackelprang, R.D. *et al.* Upregulation of IFN-stimulated genes persists beyond the transitory broad immunologic changes of acute HIV-1 infection. *iScience* **26**, 106454 (2023).
59. Fusco, D.N. *et al.* HELZ2 Is an IFN Effector Mediating Suppression of Dengue Virus. *Front Microbiol* **8**, 240 (2017).
60. Bocci, M. *et al.* Infection of Brain Pericytes Underlying Neuropathology of COVID-19 Patients. *Int J Mol Sci* **22** (2021).
61. Khan, A.O. *et al.* Preferential uptake of SARS-CoV-2 by pericytes potentiates vascular damage and permeability in an organoid model of the microvasculature. *Cardiovasc Res* **118**, 3085-3096 (2022).
62. Xu, S.W., Ilyas, I. & Weng, J.P. Endothelial dysfunction in COVID-19: an overview of evidence, biomarkers, mechanisms and potential therapies. *Acta Pharmacol Sin* **44**, 695-709 (2023).
63. Rauti, R. *et al.* Effect of SARS-CoV-2 proteins on vascular permeability. *Elife* **10** (2021).
64. Li, Y. *et al.* SARS-CoV-2 induces double-stranded RNA-mediated innate immune responses in respiratory epithelial-derived cells and cardiomyocytes. *Proc Natl Acad Sci U S A* **118** (2021).
65. Girgis, S. *et al.* Evolution of naturally arising SARS-CoV-2 defective interfering particles. *Commun Biol* **5**, 1140 (2022).
66. Al-Samkari, H. *et al.* COVID-19 and coagulation: bleeding and thrombotic manifestations of SARS-CoV-2 infection. *Blood* **136**, 489-500 (2020).
67. Xu, S.W., Ilyas, I. & Weng, J.P. Endothelial dysfunction in COVID-19: an overview of evidence, biomarkers, mechanisms and potential therapies. *Acta Pharmacol Sin*, 1-15 (2022).
68. Jiang, Z. *et al.* NOX2 and NOX5 are increased in cardiac microvascular endothelium of deceased COVID-19 patients. *Int J Cardiol* **370**, 454-462 (2023).
69. Qian, T. *et al.* Directed differentiation of human pluripotent stem cells to blood-brain barrier endothelial cells. *Sci Adv* **3**, e1701679 (2017).
70. Neal, E.H. *et al.* A Simplified, Fully Defined Differentiation Scheme for Producing Blood-Brain Barrier Endothelial Cells from Human iPSCs. *Stem Cell Reports* **12**, 1380-1388 (2019).
71. Wan, Z. *et al.* A robust vasculogenic microfluidic model using human immortalized endothelial cells and Thy1 positive fibroblasts. *Biomaterials* **276**, 121032 (2021).
72. Dobin, A. *et al.* STAR: ultrafast universal RNA-seq aligner. *Bioinformatics* **29**, 15-21 (2013).
73. Liao, Y., Smyth, G.K. & Shi, W. featureCounts: an efficient general purpose program for assigning sequence reads to genomic features. *Bioinformatics* **30**, 923-930 (2014).
74. Love, M.I., Huber, W. & Anders, S. Moderated estimation of fold change and dispersion for RNA-seq data with DESeq2. *Genome Biol* **15**, 550 (2014).
75. Stephens, M. False discovery rates: a new deal. *Biostatistics* **18**, 275-294 (2017).
76. Subramanian, A. *et al.* Gene set enrichment analysis: a knowledge-based approach for interpreting genome-wide expression profiles. *Proc Natl Acad Sci U S A* **102**, 15545-15550 (2005).
77. Finkel, Y. *et al.* The coding capacity of SARS-CoV-2. *Nature* **589**, 125-130 (2021).

## Acknowledgments

We acknowledge funding from the Wellcome-LEAP HOPE initiative, NIH (T32 EB016652), the Wyss Institute, and the Whitehead Institute. We thank the Genome Technology Core and Keck Imaging Facility at Whitehead Institute for Biomedical Research. This work was supported by NIH grant

902 U19AI131135, NIBIB grant T32 EB016652, and by a generous gift from Jim Stone. The following
903 reagent was deposited by the Centers for Disease Control and Prevention and obtained through BEI
904 Resources, NIAID, NIH: SARS-Related Coronavirus 2, Isolate USA-WA1/2020, NR-52281. This work
905 was performed in part in the Ragon Institute BSL3 core, which is supported by the NIH-funded Harvard
906 University Center for AIDS Research (P30 AI060354) and the Massachusetts Consortium on Pathogen
907 Readiness (MassCPR).
908

909 **Author Contributions**

910 A.R., A.K., R.J., and D.M designed the project. T.W. and X.G. performed the bulk RNA sequencing
911 data analysis. T.L. assisted in stem cell maintenance and differentiations. R.K. and Z.W. generated and
912 analyzed microfluidic cultures of hPSC-derived vascular cells. M.F. assisted with real-time PCR data
913 collection. L.G. facilitated work in the Ragon BSL3 facility. A.R. and A.K. analyzed all data except for
914 RNA sequencing data and prepared the manuscript. All authors discussed the results and commented
915 on the manuscript.
916

917 **Competing Interests**

918 The authors declare the following competing interests. R.J. is an advisor/co-founder of Fate
919 Therapeutics and Fulcrum Therapeutics. D.J.M. has sponsored research from Novartis, consults,
920 and/or has stock options/stock in J&J, Medicenna, Boston Scientific, Lyell, Attivare, IVIVA, Epoulosis,
921 Limax Biosciences, and Revela. The remaining authors (A.R., A.K., T.W., M.F., X.G., L.G., R.K., T.L.,
922 Z.W.) declare no competing interests.
923

924 **Table 1**

925

| | CoV-2 SMC CM | | CoV-2 PC CM | | BA5.1 SMC CM | |
|---|---|---|---|---|---|---|
| Gene Name | $Log_2FC$ | Adj. p value | $Log_2FC$ | Adj. p value | $Log_2FC$ | Adj. p value |
| MX1 | 7.46 | $2.6e^{-10}$ | 0.79 | 0.534 | 1.94 | 0.024 |
| BST2 | 8.07 | $2.15e^{-21}$ | -0.72 | 0.042 | 1.03 | 0.002 |
| DDX58 | 3.03 | $1.5e^{-10}$ | -0.69 | 0.19 | -0.61 | 0.180 |
| IRF7 | 3.11 | $3.43^{e-9}$ | -0.43 | 0.207 | 0.14 | 0.683 |
| ISG15 | 3.84 | $5.62e^{-12}$ | -0.48 | 0.087 | 0.25 | 0.852 |
| HELZ2 | 2.43 | $2.98e^{-14}$ | 1.05 | 0.044 | 2.10 | $2.55e^{-5}$ |
| OAS1 | 4.78 | 0.008 | 0.94 | 0.709 | 0.97 | 0.766 |
| EPS11 | 5.55 | $3.78e^{-10}$ | 0.39 | 0.735 | 0.16 | 0.706 |
| LY6E | 3.65 | $4.29e^{-13}$ | -0.42 | 0.135 | 0.31 | 0.429 |

926

927 **Table 1:** Differential expression of key regulators of innate immune signaling in ECs exposed to
928 conditioned media from SARS-CoV-2 infected SMCs (CoV-2 SMC CM), SARS-CoV-2 infected PC
929 (CoV-2 PC CM), or BA5.1 infected SMCs (BA5.1 SMC CM) compared to control ECs. Effect sizes were
930 estimated using DESeq2, with (two-tailed) p-values computed using the Wald statistic. A full list of
931 differentially expressed genes can be found in the source data file.

932

933

934

935

936

937
938
939 ## Figure Legends

940 **Figure 1: Derivation of hPSC derived vascular endothelial cells, smooth muscle cells, and**
941 **pericytes**. (A) Schematic of directed differentiation of hPSCs to vascular endothelial cells (ECs),
942 smooth muscle cells (SMCs) and pericytes (PCs) (Created using BioRender). (B) Bulk RNA sequencing
943 was performed on hPSC-derived ECs, PCs and SMCs. The normalized expression values of known
944 EC, PC, or SMC marker genes was quantitated over three biological replicates. The values plotted
945 represent scaled normalized expression values for each gene across samples (C) (left) Principal
946 component analysis (PCA) on bulk-RNA sequencing data from hPSC-EC, hPSC-PCs, and hPSC-
947 SMCs and primary endothelial cells (HUVECs), primary pericytes, and primary bronchial smooth
948 muscle cells (BSMCs). (right) Mural cell only PCA analysis (Primary pericytes, BSMCs, hPSC-PCs,
949 and hPSC-SMCs) (D) Expression of PECAM1, and VE-Cadherin in was quantitated by flow cytometry
950 on hPSCs or on two independent differentiations of ECs. Data points on bar graph represent values
951 from two independent differentiations. Expression of VE-Cadherin, VWF, and PECAM1 in hPSC-
952 derived ECs was observed by immunofluorescence. (E) Expression of NG2 was quantitated by flow
953 cytometry on hPSCs or on two independent differentiations of PCs. Data points on bar graph represent
954 values from two independent differentiations. Expression of PDGFR-B, and PDGFR-A was quantitated
955 by flowcytometry on HEK293 cells, human dermal fibroblast (hDF) and two independent PC
956 differentiation. Expression of SMA, PDGFR-B, and NG2 in hPSC derived PCs was observed by
957 immunofluorescence. (F) Expression of PDGFR-B or SMA was quantitated by flow cytometry on hPSCs
958 or on two independent differentiations of SMCs. Data points on bar graph represent values from two
959 independent differentiations. Expression of SMA, PDGFR-B, and NG2 in hPSC derived SMCs was
960 observed by immunofluorescence. Scale bar = 50 μm for all immunofluorescence images.
961

962 **Figure 2: hPSC derived ECs, PCs, and SMCs show selective susceptibility to SARS-CoV-2**
963 **infection.** (A) $10e^5$ hPSC-derived ECs, SMCs, and PCs were infected at an MOI of 0.1 ($10e^4$ PFU) with
964 SARS-CoV-2. The amount infectious virus released into the media at the indicated time post-infection
965 was quantitated by plaque assay in three independent experiments. Titers of EC 48 h.p.i samples were
966 below the limit of detection of 10 plaque forming units. Data are presented as mean values +/- SD. (B)
967 hPSC derived ECs, SMCs, and PCs were infected at an MOI of 0.1 with SARS-CoV-2 and fixed at 48
968 hours post-infection. Fixed cells were stained with an antibody directed against dsRNA as well as
969 antibodies directed against SMA or VE-Cadherin and imaged by immunofluorescence. The experiment
970 was performed three times with similar results. Representative images from a single experiment are
971 shown. (C) Expression of known SARS-CoV-2 receptors ACE2, TMPRSS2, and NRPP1 was
972 quantitated by bulk sequencing on hPSC-derived ECs, PCs, and SMCs. Values shown are from three
973 independent biological replicates. Scale bar = 50 μm for all immunofluorescence images.
974
975
976 **Figure 3: hPSC-derived ECs, SMCs and PCs display unique responses to SARS-CoV-2**
977 **exposure.** Bulk RNA sequencing was performed on RNA isolated from hPSC-derived vascular ECs,
978 PCs, and SMCs 48 hours after virus exposure (MOI =1). For all volcano plots effect sizes were
979 estimated using DESeq2, with (two-tailed) p-values computed using the Wald statistic. A full list of
980 differentially expressed genes can be found in the Source Data file. (A) Volcano plots showing
981 differential gene expression in ECs exposed to live SARS-CoV-2 compared to control uninfected ECs.
982 Gene set enrichment analysis (GSEA)[76] was performed on differentially expressed genes to analyze
983 the transcriptional response to infection. Dot plots show gene-sets from the Hallmark collection[34] of the
984 MSigDB that were enriched (FDR < 0.05). (B) Volcano plots showing differential gene expression in
985 SMCs exposed to live SARS-CoV-2 compared to control uninfected SMCs. GSEA was performed on
986 differentially expressed genes to analyze the transcriptional response to infection. Dot plots show gene-
987 sets from the Hallmark collection[34] of the MSigDB that were enriched (FDR < 0.05). (C) Volcano plots

988 showing differential gene expression in PCs exposed to live SARS-CoV-2 compared to control
989 uninfected PCs. GSEA was performed on differentially expressed genes to analyze the transcriptional
990 response to infection. Dot plots show gene-sets from the Hallmark collection of the MSigDB that were
991 enriched (FDR < 0.05).
992
993 **Figure 4: SARS-CoV-2 exposure induces reactive oxygen species production and decreases**
994 **barrier function of hPSC-derived ECs.** (A) ECs were mock-infected or exposed to live or heat-
995 inactivated SARS-CoV-2 for 48 hours (MOI=1). CellROX green reagent was added at a final
996 concentration of 5 μM and incubated for 30 minutes and cells were analyzed by fluorescence
997 microscopy. Green fluorescent signal showed the ROS-mediated oxidation of the reagent. The
998 fluorescence intensity was measured for five cells for each condition for three independent
999 experiments. For each experiment the value plotted is the average fold change in florescence intensity
000 relative to mock-infected cells for that experiment. Conditions were compared using a one-way ANOVA
001 with Dunnett's multiple comparisons test, with a single pooled variance. (B) Representative images of
002 CellRox staining at 48 hours post-infection from a single experiment (Scale bar = 50 μm). (C)
003 Transcytosis of FITC–tagged 10-kDa dextran across a monolayer hPSC-derived ECs. ECs were plated
004 in transwells and infected with SARS-CoV-2 (MOI=1) or mock infected for 48 hours. FITC-dextran was
005 added to the upper chamber and the fluorescence intensity of media the lower chamber was quantitated
006 four hours after FITC-dextran addition. Three independent experiments were performed. All results are
007 expressed as a fold change relative to the average value for mock infected ECs. Conditions were
008 compared using an unpaired t-test.
009
010 **Figure 5: SMCs exposed to SARS-CoV-2 release factors that alter EC gene expression (A)**
011 Schematic of the experiment examining the effect of SMC-secreted factors on ECs (Created using
012 BioRender). (B-E) Bulk RNA sequencing was performed on RNA isolated from ECs 48 hours after
013 exposure to SMC conditioned media. For all volcano plots effect sizes were estimated using DESeq2,

014 with (two-tailed) p-values computed using the Wald statistic. A full list of differentially expressed genes
015 can be found in the source data file. (B) Volcano plot of differentially expressed genes in ECs exposed
016 to media from SARS-CoV-2 infected SMCs (*CoV-2 SMC CM*) compared to control ECs *(Control)*. (C)
017 Volcano plot of differentially expressed genes in ECs treated with media from SMCs exposed to heat-
018 inactivated SARS-CoV-2 *(HI SMC CM)* compared to control ECs *(Control)*. (D) GSEA results of ECs
019 treated with media from SARS-CoV-2 infected SMCs compared to control ECs (*Media Transfer*) plotted
020 together with GSEA results for ECs exposed to live SARS-CoV-2 compared to control ECs (*Direct*
021 *Infection*) (E) GSEA results of ECs treated with media from SMCs exposed to heat-inactivated SARS-
022 CoV-2 compared to control ECs (*Media Transfer*) plotted together with GSEA results for ECs exposed
023 to live SARS-CoV-2 compared to control ECs (*Direct Infection*). In (D) and (E), the Hallmark collection[34]
024 of gene-sets from the MSigDB was used and gene-sets were plotted only when FDR < 0.05 for
025 enrichment in at least one of the between-condition comparisons.

026

027 **Figure 6: SARS-CoV-2 exposed SMCs release factors that promote clotting and reduce barrier**
028 **function in ECs.** (A, B) Bulk RNA sequencing was performed on RNA isolated from ECs 48 hours after
029 exposure to SMC-conditioned media (Figure 4A) (A) Volcano plot for differential gene expression in
030 ECs exposed to media from SARS-CoV-2 infected SMCs (*CoV-2 SMC CM*) compared to control ECs
031 *(Control)*. For all volcano plots effect sizes were estimated using DESeq2, with (two-tailed) p-values
032 computed using the Wald statistic. A full list of differentially expressed genes can be found in the source
033 data file. (B) Volcano plot for differential gene expression in ECs exposed to media from SMCs exposed
034 to heat-inactivated SARS-CoV-2 *(HI SMC CM)* compared to control ECs *(Control)*. In both (A) and (B),
035 genes highlighted in red correspond to the "coagulation" gene-set from the Hallmark collection[34] of the
036 MSigDB, with GSEA "leading edge" genes labeled by name. (C-E) ECs were exposed to media from
037 SARS-CoV-2 infected SMCs (*CoV-2 SMC Exposed*) or exposed to media from mock infected SMCs
038 *(Mock SMC Exposed)* for 48 hours. (C) The amount of SERPINE1(PAI-1) ECs released into the media
039 48 hours after CM exposure was quantitated by ELISA. Media was collected from three independent
040 experiments and analyzed in parallel. Bar graph is the average value for each condition and data points

041 show the individual values from each experiment. Error bar shows +/- SD. Conditions were compared
042 using an unpaired t-test. (D) The amount of von Willibrand Factor (vWF) ECs released into the media
043 48 hours after CM exposure was quantitated by ELISA. Media was collected from three independent
044 experiments and analyzed in parallel. Bar graph is the average value for each condition and data points
045 show the individual values from each experiment. Error bar shows +/- SD. Conditions were compared
046 using an unpaired t-test. (E) Transcytosis of FITC–tagged 10-kDa dextran across a monolayer hPSC-
047 derived ECs. ECs were plated in transwells and exposed to media from SARS-CoV-2 infected SMCs
048 (*CoV-2 SMC CM*) or media from mock infected SMCs (*Mock SMC Exposed*) for 48 hours. FITC-dextran
049 was added to the upper chamber and the fluorescence intensity of media the lower chamber was
050 quantitated four hours after FITC-dextran addition. Three independent experiments were performed.
051 All results are expressed as a fold change relative to the average value for mock-exposed ECs. Each
052 dot represents the value from an independent experiment and lines show mean value across all three
053 experiments. Conditions were compared using an unpaired t-test.
054
055 **Figure 7: SARS-CoV-2 infection of SMCs increases tissue factor expression and activity**. (A)
056 SMCs were infected with SARS-CoV-2 for 48 hours (MOI=1) and stained with antibodies against
057 dsRNA and tissue factor. Staining of actin with phalloidin was included to mark cell bodies. (B)
058 Immunofluorescence staining for tissue factor in hPSC-derived SMCs exposed to either live or heat-
059 inactivated (HI) SARS-CoV-2 or uninfected control hPSC-derived SMCs. Cells were fixed at 48 hours
060 post-infection. Scale bar = 200 μm. The experiment was performed three times with similar results. (C)
061 Quantitation of tissue factor staining shown in (B). Bar graph shows mean value and error bar shows
062 95% confidence interval. Conditions were compared using a one-way ANOVA with Dunnett's multiple
063 comparisons test, with a single pooled variance. (D)Tissue factor activity in cell lysate from SMCs
064 exposed to live SARS-CoV-2 or HI SARS-CoV-2 (MOI=1) for 48 hours was quantitated by ELISA and
065 is reported as a percent increase compared to control uninfected SMCs. Scale bar = 50 μm for all
066 immunofluorescence images. Activity levels were analyzed for three independent experiments for live

067 SARS-CoV-2 treatment and five independent experiments for HI SARS-CoV-2. Levels were normalized
068 to the average value for control SMCs for that experiment. Bar graph shows mean value and error bar
069 shows 95% confidence interval. Each condition was compared to 100% activity for control SMCs using
070 a one sample t test.
071
072
073
074
075
076
077
078
079
080
081
082
083
084
085
086
087

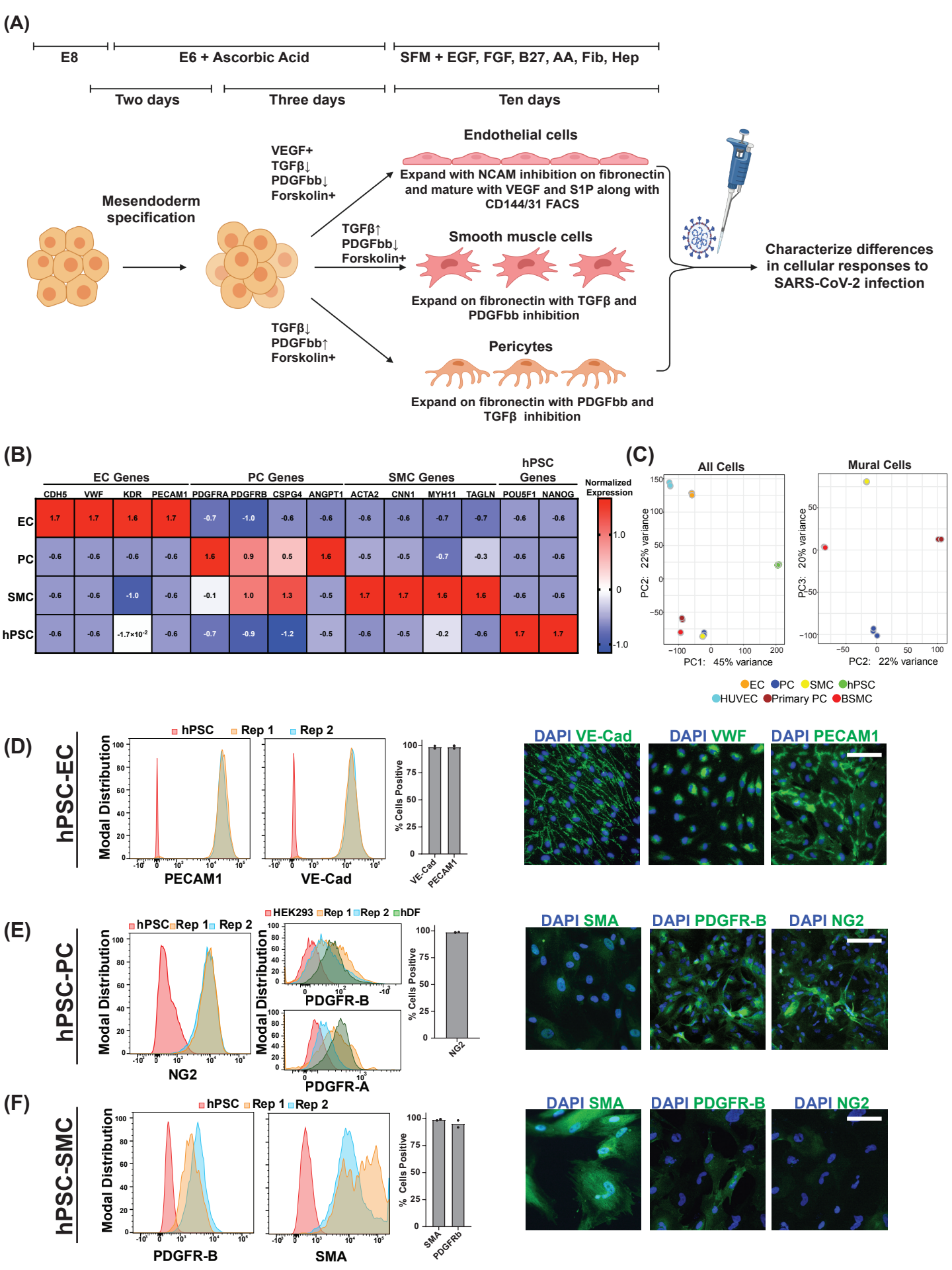
(A)
E8
E6 + Ascorbic Acid
SFM + EGF, FGF, B27, AA, Fib, Hep
Two days
Three days
Ten days
Mesendoderm specification
VEGF+
TGFβ↓
PDGFbb↓
Forskolin+
Endothelial cells
Expand with NCAM inhibition on fibronectin and mature with VEGF and S1P along with CD144/31 FACS
TGFβ↑
PDGFbb↓
Forskolin+
Smooth muscle cells
Expand on fibronectin with TGFβ and PDGFbb inhibition
TGFβ↓
PDGFbb↑
Forskolin+
Pericytes
Expand on fibronectin with PDGFbb and TGFβ inhibition
Characterize differences in cellular responses to SARS-CoV-2 infection
(B)
EC Genes
PC Genes
SMC Genes
hPSC Genes
CDH5 VWF KDR PECAM1 PDGFRA PDGFRB CSPG4 ANGPT1 ACTA2 CNN1 MYH11 TAGLN POU5F1 NANOG
EC 1.7 1.7 1.6 1.7 -0.7 -1.0 -0.6 -0.6 -0.6 -0.6 -0.7 -0.7 -0.6 -0.6
PC -0.6 -0.6 -0.6 -0.6 1.6 0.9 0.5 1.6 -0.5 -0.5 -0.7 -0.3 -0.6 -0.6
SMC -0.6 -0.6 -1.0 -0.6 -0.1 1.0 1.3 -0.5 1.7 1.7 1.6 1.6 -0.6 -0.6
hPSC -0.6 -0.6 -1.7×10-2 -0.6 -0.7 -0.9 -1.2 -0.5 -0.6 -0.5 -0.2 -0.6 1.7 1.7
Normalized Expression
1.0
0
-1.0
(C)
All Cells
Mural Cells
PC2: 22% variance
PC1: 45% variance
PC3: 20% variance
PC2: 22% variance
EC PC SMC hPSC
HUVEC Primary PC BSMC
(D)
hPSC-EC
hPSC Rep 1 Rep 2
Modal Distribution
PECAM1
VE-Cad
% Cells Positive
VE-Cad PECAM1
DAPI VE-Cad
DAPI VWF
DAPI PECAM1
(E)
hPSC-PC
hPSC Rep 1 Rep 2
HEK293 Rep 1 Rep 2 hDF
Modal Distribution
NG2
PDGFR-B
PDGFR-A
% Cells Positive
NG2
DAPI SMA
DAPI PDGFR-B
DAPI NG2
(F)
hPSC-SMC
hPSC Rep 1 Rep 2
Modal Distribution
PDGFR-B
SMA
% Cells Positive
SMA PDGFRb
DAPI SMA
DAPI PDGFR-B
DAPI NG2

(A)

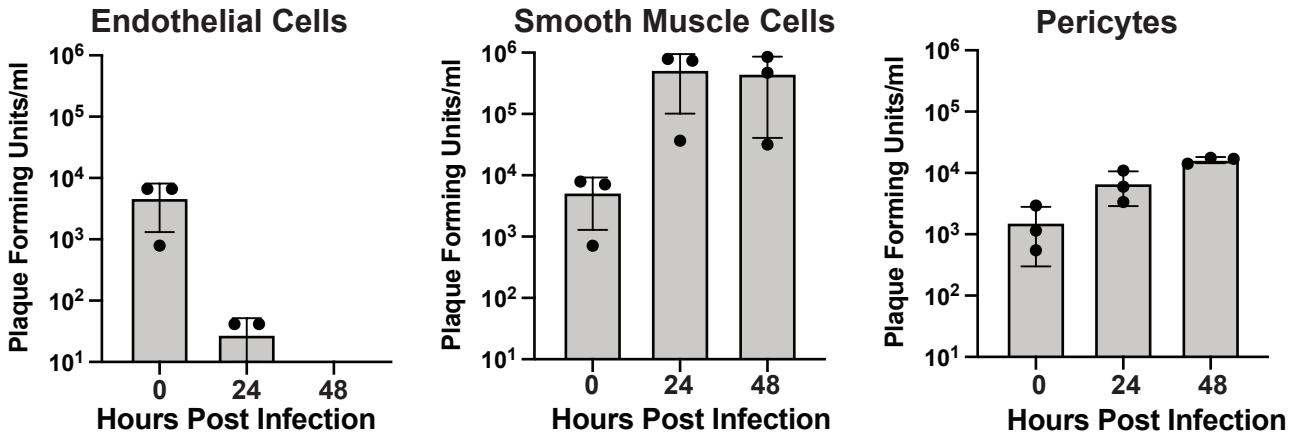
Endothelial Cells
Smooth Muscle Cells
Pericytes
Plaque Forming Units/ml
$10^1$
$10^2$
$10^3$
$10^4$
$10^5$
$10^6$
0
24
48
Hours Post Infection

(B)

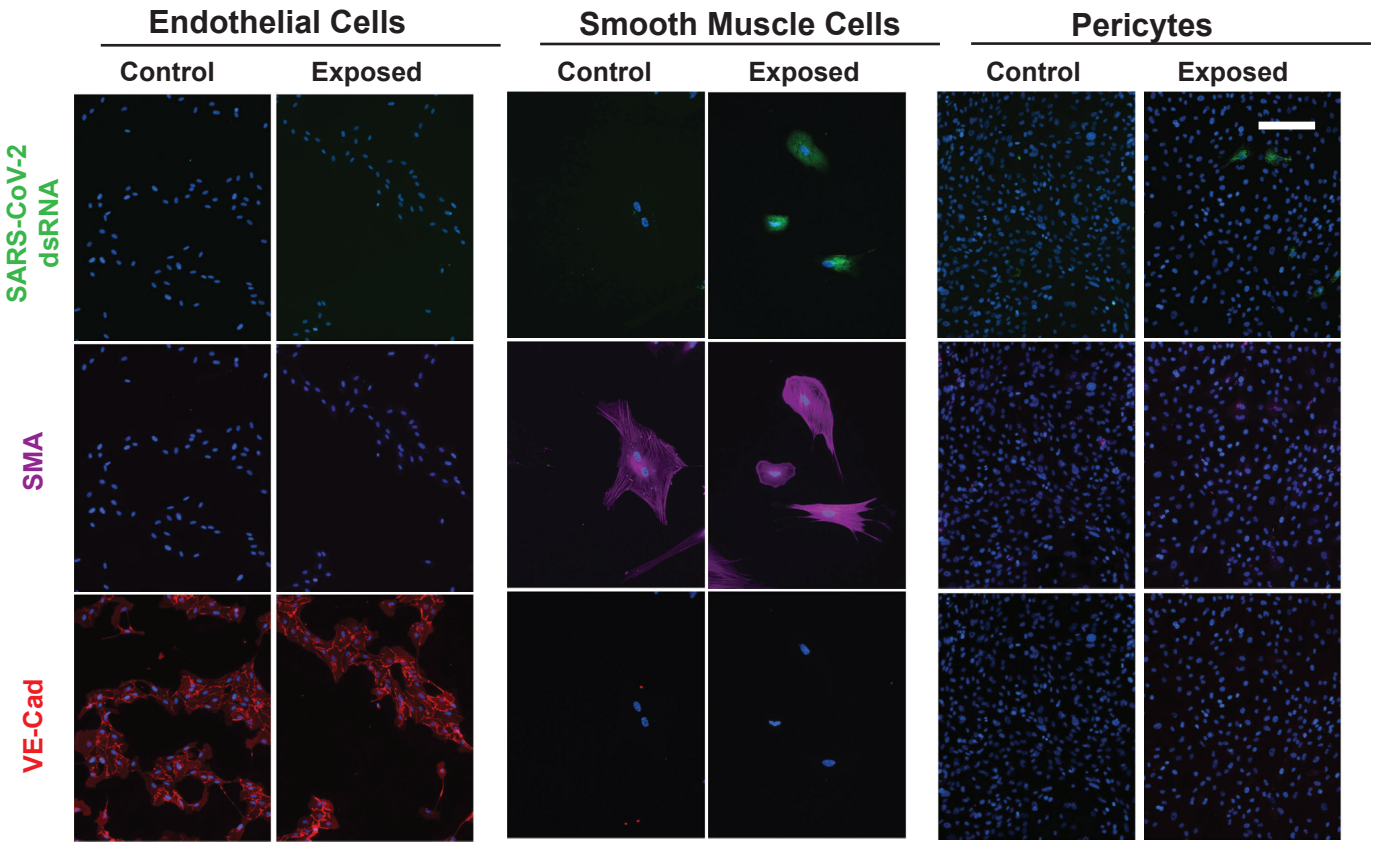
Endothelial Cells
Smooth Muscle Cells
Pericytes
Control
Exposed
SARS-CoV-2 dsRNA
SMA
VE-Cad

(C)

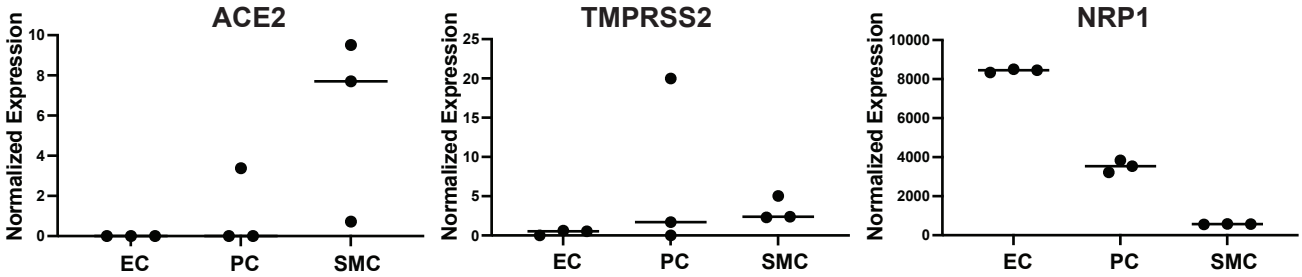
ACE2
TMPRSS2
NRP1
Normalized Expression
EC
PC
SMC

(A)

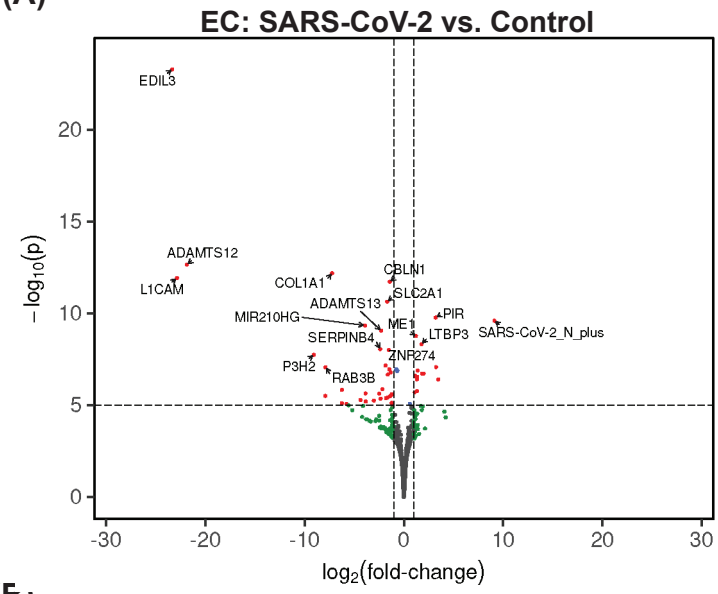
EC: SARS-CoV-2 vs. Control
EDIL3
ADAMTS12
L1CAM
COL1A1
CBLN1
SLC2A1
ADAMTS13
MIR210HG
ME1
PIR
LTBP3
SARS-CoV-2_N_plus
SERPINB4
ZNF274
P3H2
RAB3B
$-\log_{10}(p)$
$\log_2$(fold-change)

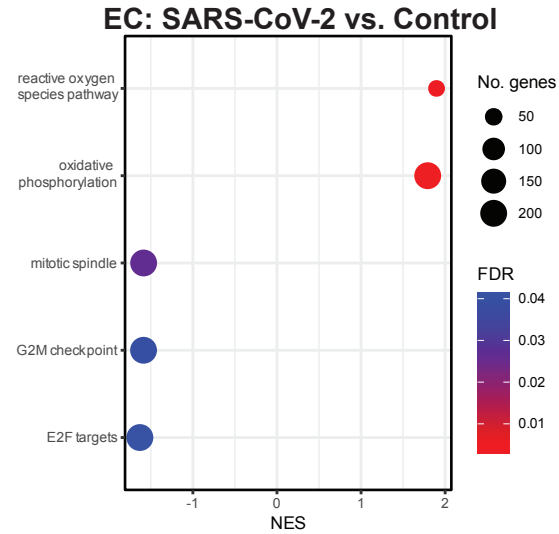
EC: SARS-CoV-2 vs. Control
reactive oxygen species pathway
oxidative phosphorylation
mitotic spindle
G2M checkpoint
E2F targets
NES
No. genes
50
100
150
200
FDR
0.04
0.03
0.02
0.01

(B)

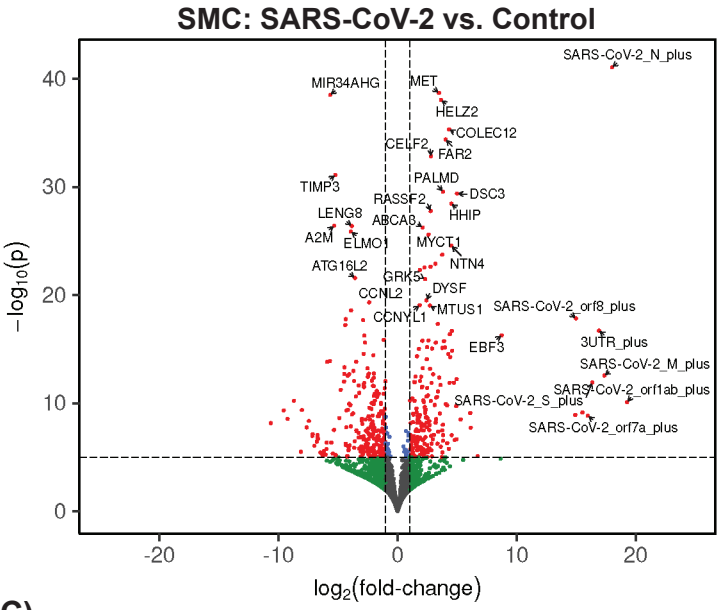
SMC: SARS-CoV-2 vs. Control
SARS-CoV-2_N_plus
MIR34AHG
MET
HELZ2
COLEC12
CELF2
FAR2
PALMD
TIMP3
DSC3
RASSF2
HHIP
LENG8
ABCA8
A2M
ELMO1
MYCT1
ATG16L2
NTN4
GRK5
DYSF
CCNL2
MTUS1
SARS-CoV-2_orf8_plus
CCNYL1
EBF3
3UTR_plus
SARS-CoV-2_M_plus
SARS-CoV-2_orf1ab_plus
SARS-CoV-2_S_plus
SARS-CoV-2_orf7a_plus
$-\log_{10}(p)$
$\log_2$(fold-change)

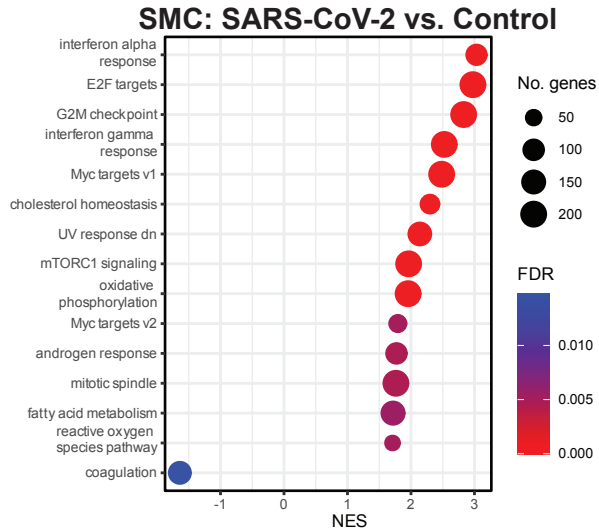
SMC: SARS-CoV-2 vs. Control
interferon alpha response
E2F targets
G2M checkpoint
interferon gamma response
Myc targets v1
cholesterol homeostasis
UV response dn
mTORC1 signaling
oxidative phosphorylation
Myc targets v2
androgen response
mitotic spindle
fatty acid metabolism
reactive oxygen species pathway
coagulation
NES
No. genes
50
100
150
200
FDR
0.010
0.005
0.000

(C)

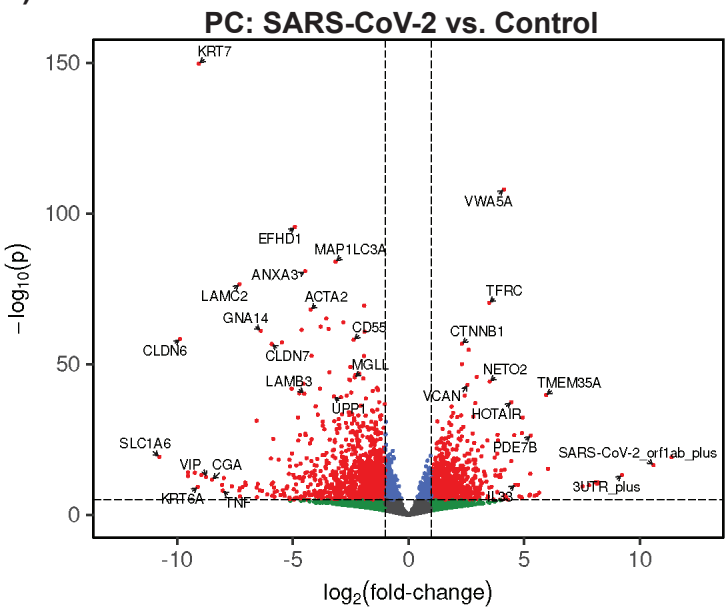
PC: SARS-CoV-2 vs. Control
KRT7
VWA5A
EFHD1
MAP1LC3A
ANXA3
TFRC
LAMC2
ACTA2
GNA14
CD55
CTNNB1
CLDN6
CLDN7
MGLL
NETO2
LAMB3
TMEM35A
VCAN
UPP1
HOTAIR
SLC1A6
PDE7B
SARS-CoV-2_orf1ab_plus
VIP
CGA
3UTR_plus
KRT6A
TNF
IL36
$-\log_{10}(p)$
$\log_2$(fold-change)

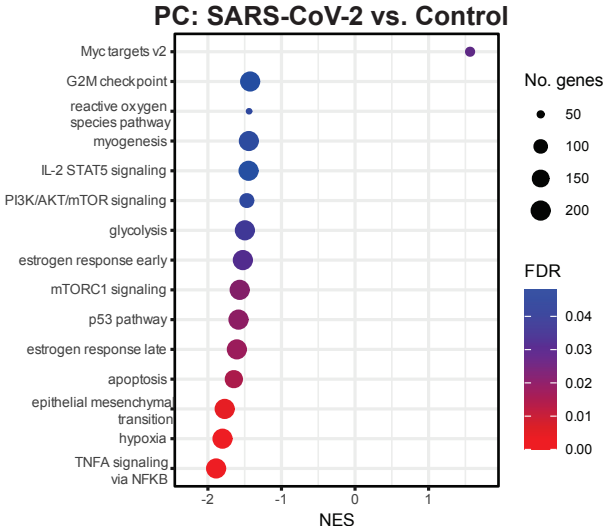
PC: SARS-CoV-2 vs. Control
Myc targets v2
G2M checkpoint
reactive oxygen species pathway
myogenesis
IL-2 STAT5 signaling
PI3K/AKT/mTOR signaling
glycolysis
estrogen response early
mTORC1 signaling
p53 pathway
estrogen response late
apoptosis
epithelial mesenchymal transition
hypoxia
TNFA signaling via NFKB
NES
No. genes
50
100
150
200
FDR
0.04
0.03
0.02
0.01
0.00

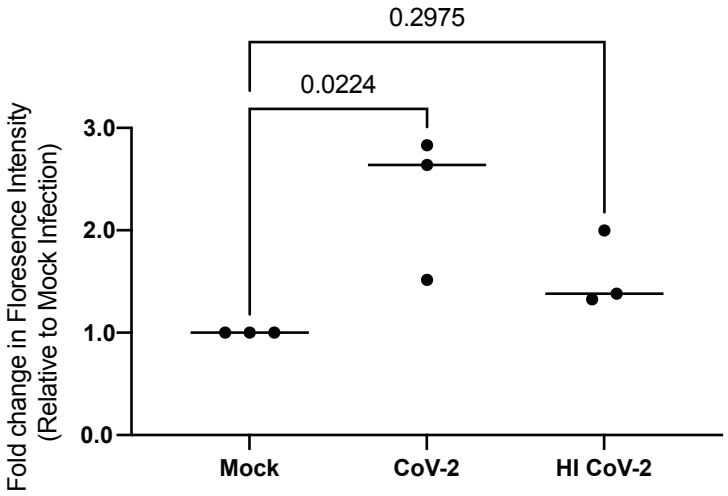
(A)
0.2975
0.0224
Fold change in Floresence Intensity
(Relative to Mock Infection)
3.0
2.0
1.0
0.0
Mock
CoV-2
HI CoV-2

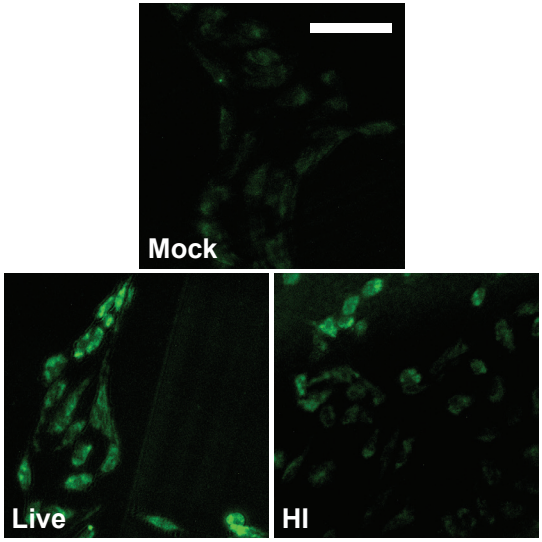
(B)
Mock
Live
HI

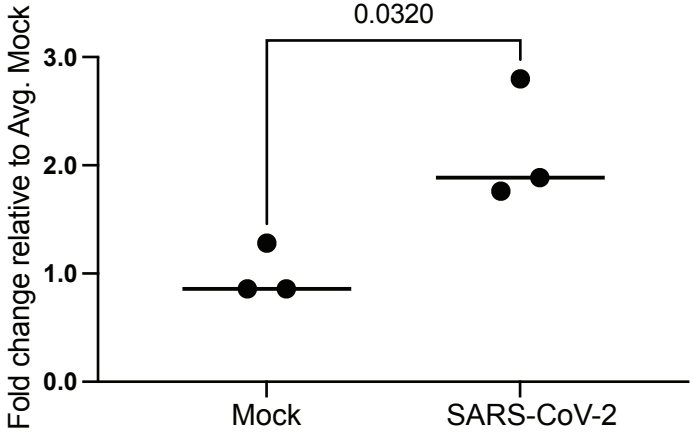
(C)
EC Permeability: FITC Dextran
0.0320
Fold change relative to Avg. Mock
3.0
2.0
1.0
0.0
Mock
SARS-CoV-2

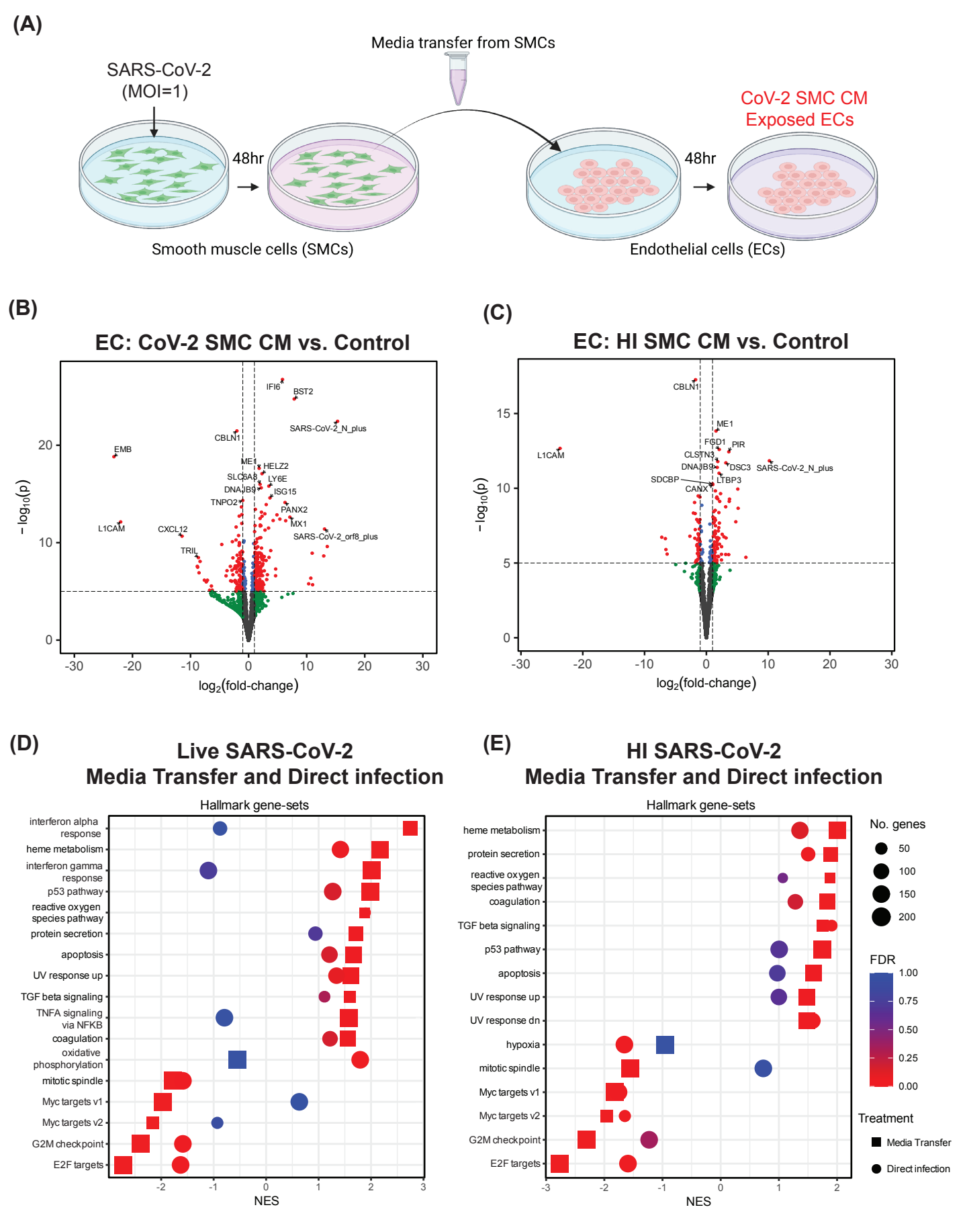
(A)
Media transfer from SMCs
SARS-CoV-2
(MOI=1)
48hr
48hr
CoV-2 SMC CM
Exposed ECs
Smooth muscle cells (SMCs)
Endothelial cells (ECs)
(B)
EC: CoV-2 SMC CM vs. Control
IFI6
BST2
SARS-CoV-2_N_plus
CBLN1
EMB
ME1
HELZ2
SLC6A8
LY6E
DNAJB9
ISG15
TNPO2
PANX2
MX1
L1CAM
CXCL12
SARS-CoV-2_orf8_plus
TRIL
$-\log_{10}(p)$
$\log_2$(fold-change)
(C)
EC: HI SMC CM vs. Control
CBLN1
ME1
FGD1
PIR
L1CAM
CLSTN3
DNAJB9
DSC3
SARS-CoV-2_N_plus
SDCBP
LTBP3
CANX
$-\log_{10}(p)$
$\log_2$(fold-change)
(D)
Live SARS-CoV-2
Media Transfer and Direct infection
Hallmark gene-sets
interferon alpha response
heme metabolism
interferon gamma response
p53 pathway
reactive oxygen species pathway
protein secretion
apoptosis
UV response up
TGF beta signaling
TNFA signaling via NFKB
coagulation
oxidative phosphorylation
mitotic spindle
Myc targets v1
Myc targets v2
G2M checkpoint
E2F targets
NES
(E)
HI SARS-CoV-2
Media Transfer and Direct infection
Hallmark gene-sets
heme metabolism
protein secretion
reactive oxygen species pathway
coagulation
TGF beta signaling
p53 pathway
apoptosis
UV response up
UV response dn
hypoxia
mitotic spindle
Myc targets v1
Myc targets v2
G2M checkpoint
E2F targets
NES
No. genes
50
100
150
200
FDR
1.00
0.75
0.50
0.25
0.00
Treatment
Media Transfer
Direct infection

Figure 6

(A)

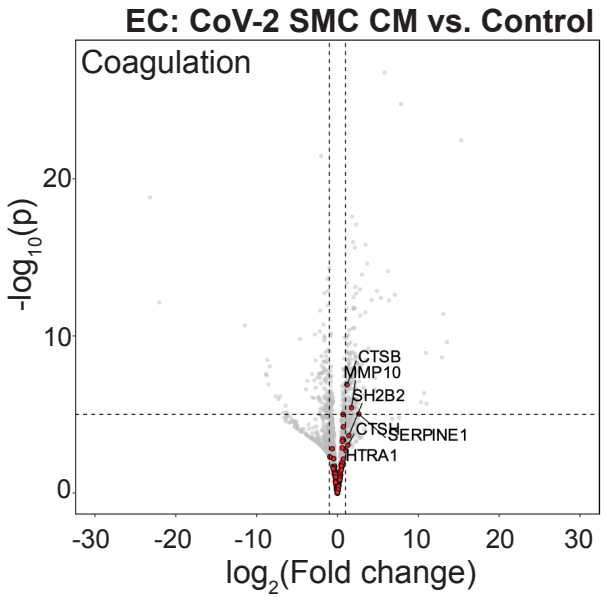


(B)

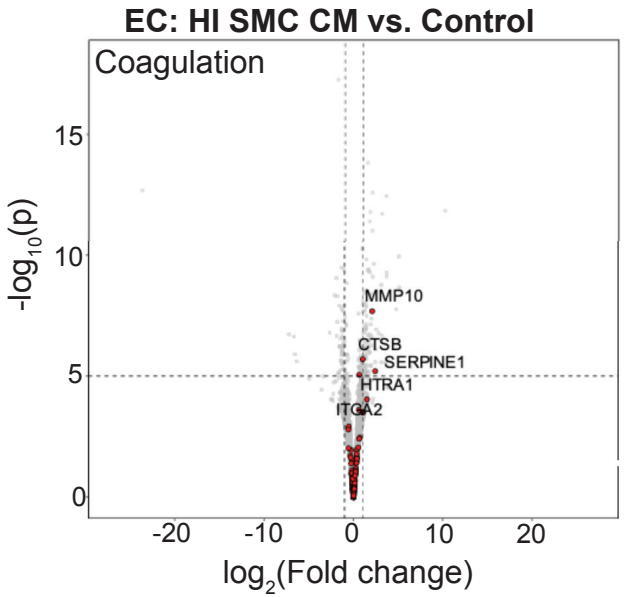


(C)

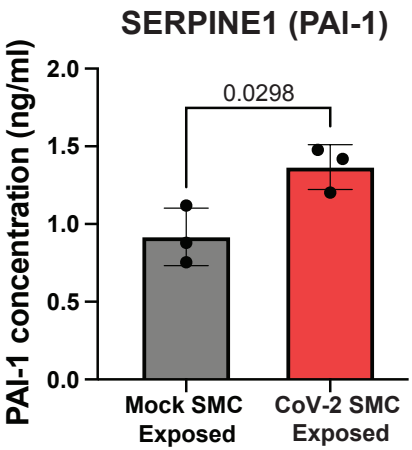


(D)

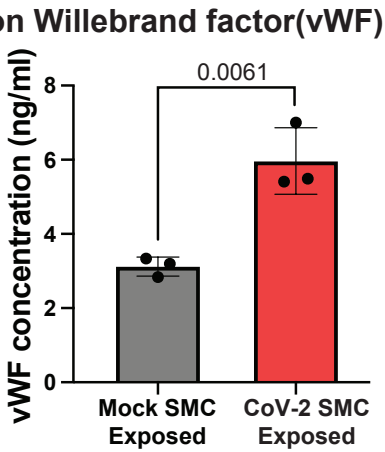


(E)

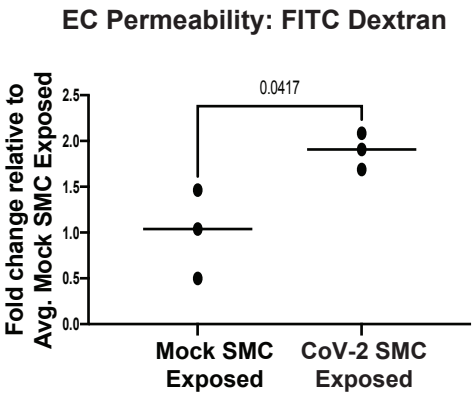

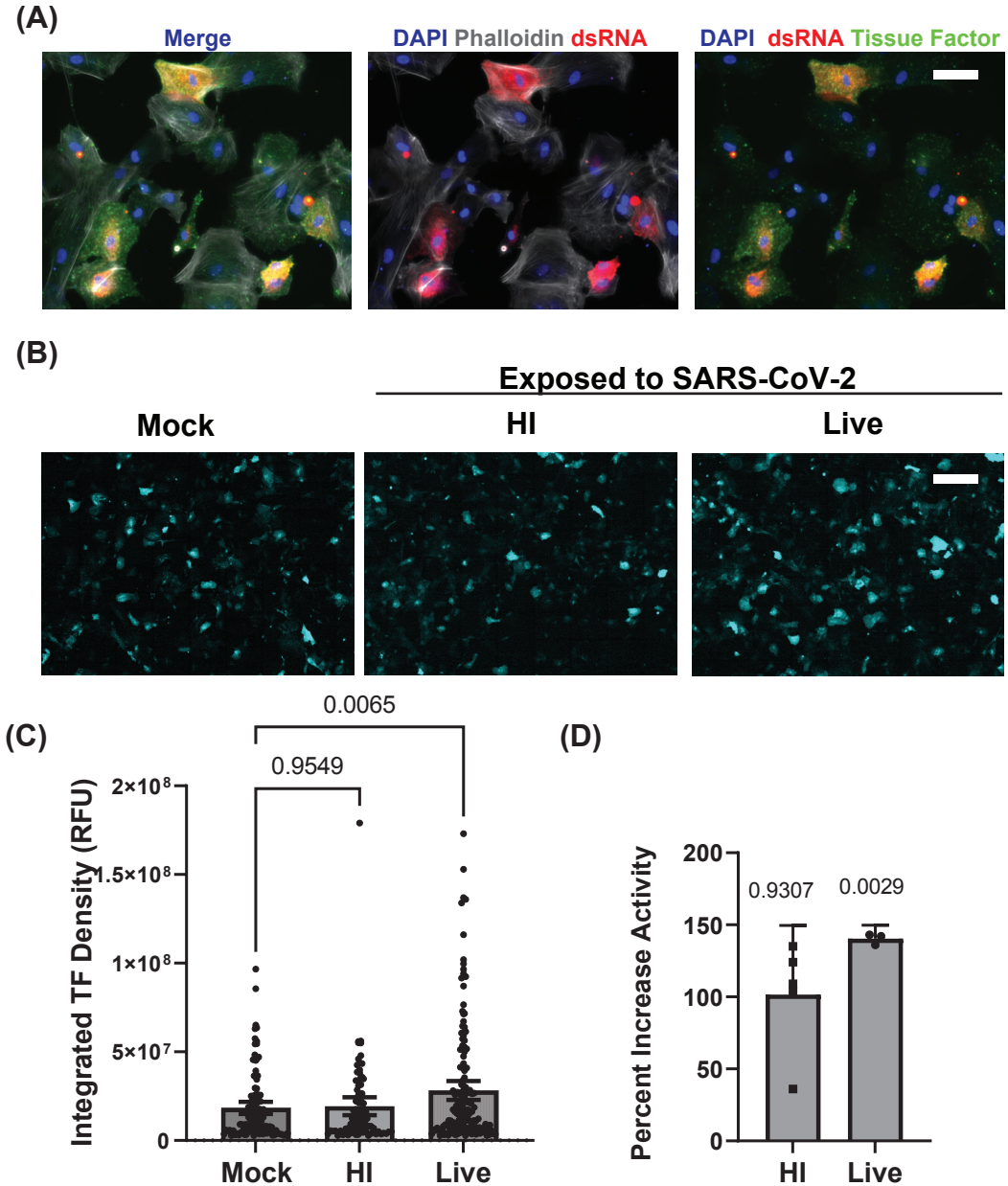
(A)
Merge
DAPI Phalloidin dsRNA
DAPI dsRNA Tissue Factor
(B)
Exposed to SARS-CoV-2
Mock
HI
Live
(C)
0.0065
0.9549
Integrated TF Density (RFU)
2×10^8
1.5×10^8
1×10^8
5×10^7
0
Mock
HI
Live
(D)
Percent Increase Activity
200
150
100
50
0
0.9307
0.0029
HI
Live